

Four jet event shapes in electron-positron annihilation

J. M. Campbell, M. A. Cullen and E. W. N. Glover

Department of Physics, University of Durham, Durham DH1 3LE, England

Abstract

We report next-to-leading order perturbative QCD predictions of 4 jet event shape variables for the process $e^+e^- \rightarrow 4$ jets obtained using the general purpose Monte Carlo **EERAD2**. This program is based on the known ‘squared’ one loop matrix elements for the virtual $\gamma^* \rightarrow 4$ parton contribution and squared matrix elements for 5 parton production. To combine the two distinct final states numerically we present a hybrid of the commonly used subtraction and slicing schemes based on the colour antenna structure of the final state which can be readily applied to other processes. We have checked that the numerical results obtained with **EERAD2** are consistent with next-to-leading order estimates of the distributions of previously determined four jet-like event variables. We also report the next-to-leading order scale independent coefficients for some previously uncalculated observables; the light hemisphere mass, narrow jet broadening, Aplanarity and the 4 jet transition variables with respect to the JADE and Geneva jet finding algorithms. For each of these observables, the next-to-leading order corrections calculated at the physical scale significantly increase the rate compared to leading order (the K factor is approximately 1.5 – 2). With the exception of the 4 jet transition variables, the published DELPHI data lies well above the $\mathcal{O}(\alpha_s^3)$ predictions. The renormalisation scale uncertainty is still large and in most cases the data prefers a scale significantly smaller than the physical scale. This situation is reminiscent of that for three jet shape variables, and should be improved by the inclusion of power corrections and resummation of large infrared logarithms.

1 Introduction

Electron-positron colliders, in particular those at both LEP and SLAC, have provided much precision data with which to probe the structure of QCD. This is particularly valuable data because the strong interactions occur only in the final state and are not entangled with the parton density functions associated with beams of hadrons. In addition to measuring multi-jet production rates, more specific information about the topology of the events can be extracted. To this end, many variables have been introduced which characterize the hadronic structure of an event. For example, we can ask how planar or how collimated an event is. In general, a variable is described as n jet-like if it vanishes for a final state configuration of $n - 1$ hadrons. With the precision data from LEP and SLC, experimental distributions for such event shape variables have been studied and have been compared where possible with theoretical calculations.

Generally speaking, leading order (LO) predictions successfully predict the general features of distributions, but can be improved by resumming kinematically-dominant logarithms, by including more perturbative information or both. A next-to-leading order (NLO) treatment of three-jet like variables was first performed in [1, 2] and systematically completed in [3]. Armed with such calculations, one can extract a value for the strong coupling α_s either directly from the event shape distributions [4] or from the energy dependence of their average value [5]. Alternatively, one can study the group parameters of the gauge theory of the strong interactions [6], though for three jet observables, the gluon-gluon coupling (proportional to C_A) occurs first at NLO.

Recent calculations of the relevant one-loop four parton matrix elements for $\gamma^* \rightarrow 4$ partons [7] and $e^+e^- \rightarrow 4$ partons [8], together with the known tree-level five parton matrix elements [9] have enabled the phenomenology of four-jet production to be studied at next-to-leading order. So far, two groups have used these matrix elements to construct general purpose Monte Carlo programs for four jet-like quantities **MENLO** **PARC** [10] and **DEBRECEN** [11], which have been used to measure the four jet fraction R_4 and a variety of event shape distributions [11]. We note that four jet production is sensitive to the casimir structure of QCD [12, 8] and four jet events may be used to constrain the allowed values of C_F , C_A and T_R [13] by examining the angles between the jets [14]. One may also place next-to-leading order bounds on the possible presence of the elusive light gluino present in many supersymmetric models [15].

Any such Monte Carlo program must suitably combine the virtual four parton and real five parton pieces of the cross section. That is,

$$\sigma_{\text{NLO}} = \int d\sigma_4 + \int d\sigma_5 = \int dPS_4 |\mathcal{M}_4|^2 + \int dPS_5 |\mathcal{M}_5|^2, \quad (1.1)$$

where the n -parton contributions $d\sigma_n$ are integrals over the n -parton phase-space dPS_n . Both integrals are separately divergent, and contain both infrared and ultraviolet singularities. The ultraviolet poles are removed by renormalisation, however the soft and collinear infrared poles are only cancelled when the virtual graphs are combined with the bremsstrahlung process and one must provide a means to cancel the infrared singularities caused

by two particles becoming collinear or one soft. Although the cancellation of infrared poles can be done analytically for simple processes, for complicated processes, it is necessary to resort to numerical techniques. A variety of methods - known as subtraction [1, 16, 17], slicing [2, 18] and hybrid subtraction [19] - are in general use, and variations of the subtraction formalism have been implemented in [10, 11]. Here we report on results obtained using a third numerical implementation of these matrix elements to compute generic infrared safe four jet observables. We call this program **EERAD2** [20] and it is based on the ‘squared’ one-loop matrix elements for $\gamma^* \rightarrow 4$ partons of [7] together with squared tree level matrix elements for $\gamma^* \rightarrow 5$ partons. To isolate and cancel the infrared singularities, we use a hybrid approach that contains elements of both slicing and subtraction methods. In particular, we use an antenna factorisation where two (colour connected) hard partons radiate a third that may be unresolved. This is necessarily a rather technical subject and it is detailed in the appendix.

For the bulk of the paper we are more concerned with the phenomenology of four jet-like shape variables and, in particular, we extend the set of variables that have been computed at $\mathcal{O}(\alpha_s^3)$.¹ To be precise, we present next-to-leading order coefficients for the differential distributions of the narrow jet broadening, light hemisphere mass, Aplanarity and the jet transition variable for the JADE and Geneva jet algorithms. To compare with previous results, we also consider the thrust minor, D parameter and the jet transition variable for the Durham jet algorithm as well as the four jet rate as a function of the jet resolution parameter y_{cut} .

In section 2, we give the definitions of the relevant four jet shape variables and review the structure of the perturbative predictions. Section 3 shows the consistency of our program, by reproducing the known four-jet fraction and D parameter distributions. The main results are reported in section 4 and comparisons with experimental data follow in section 5, where we also discuss how we might optimize our perturbative input by choice of a suitable renormalization scale. Conclusions are summarized in section 6. Finally, a more detailed discussion of our method for cancellation of the infrared singularities is reserved for the Appendix.

¹Some of the results presented here have been reported in [21].

2 Four jet event shapes

The sorts of variables we are interested in are four jet-like, since they can only be non-zero for final states in which there are four or more particles. They usually rely on the hadronic final state having some volume and, when the event is coplanar, some observables like the D parameter are identically zero.

2.1 Definition of Variables

In the following definitions, the sums run over all N final state particles, $k = 1, \dots, N$. \vec{p}_k is the three-momentum of particle k in the c.m. frame, with components p_k^i , $i = 1, 2, 3$.

(a) C and D parameters [22].

We first construct the linear momentum tensor,

$$\Theta^{ij} = \frac{\sum_k \frac{p_k^i p_k^j}{|\vec{p}_k|}}{\sum_k |\vec{p}_k|}, \quad (2.1)$$

with eigenvalues λ_i for $i = 1, 2, 3$. The normalisation is such that $\sum_i \lambda_i = 1$. For planar events one of the eigenvalues is zero. The C and D parameters are defined by,

$$D = 27\lambda_1\lambda_2\lambda_3, \quad (2.2)$$

and,

$$C = 3(\lambda_1\lambda_2 + \lambda_2\lambda_3 + \lambda_3\lambda_1). \quad (2.3)$$

D can only be non-zero for non-planar four (or more) parton events, while three parton events may produce $0 \leq C \leq 0.75$. Only the region $C > 0.75$ should be considered four jet-like.

(b) Thrust minor, T_{minor} [23].

We first define the thrust, major and minor axes $(\vec{n}_1, \vec{n}_2, \vec{n}_3)$ by,

$$T_i = \max_{\vec{n}_i} \frac{\sum_k |\vec{p}_k \cdot \vec{n}_i|}{\sum_k |\vec{p}_k|}, \quad (2.4)$$

where \vec{n}_2 is constrained by $\vec{n}_1 \cdot \vec{n}_2 = 0$. and $\vec{n}_3 = \vec{n}_1 \times \vec{n}_2$.

(c) Light hemisphere mass, M_L^2/s .

The event is separated into two hemispheres H_1, H_2 divided by the plane normal to the thrust axis \vec{n}_1 , as defined above. Particles that satisfy $\vec{p}_i \cdot \vec{n}_1 > 0$ are assigned to hemisphere H_1 , while all other particles are in H_2 . Then,

$$\frac{M_L^2}{s} = \frac{1}{s} \cdot \min_{i=1,2} \left(\sum_{\vec{p}_k \in H_i} p_k \right)^2. \quad (2.5)$$

Note that this is the common modification of the original definition suggested by Clavelli [24].

- (d) Narrow jet broadening, B_{\min} [25].

Using the same division into hemispheres as above, we define,

$$B_{\min} = \min_{i=1,2} \frac{\sum_{\vec{p}_k \in H_i} |\vec{p}_k \times \vec{n}|}{2 \sum_k |\vec{p}_k|}. \quad (2.6)$$

- (e) Aplanarity, A [26].

Here we consider the eigenvalues, $\lambda_1 \geq \lambda_2 \geq \lambda_3$ of the quadratic momentum tensor,

$$\Phi^{ij} = \frac{\sum_k p_k^i p_k^j}{\sum_k |\vec{p}_k|^2}. \quad (2.7)$$

Aplanarity is defined by,

$$A = \frac{3}{2} \lambda_3, \quad (2.8)$$

which is clearly zero for planar three particle events.

- (f) Jet transition variable y_4^S .

The y_4^S variable denotes the value of the jet resolution parameter y_{cut} at which an event changes from a four jet event to a three jet event where the jets are defined according to algorithm S . We consider three algorithms, the JADE algorithm ($S = J$) [27], the Durham algorithm ($S = D$) [28] and the Geneva algorithm ($S = G$) [29]. The jet-finding measures for each of these three algorithms are as follows,

$$\begin{aligned} y_{ij}^J &= \frac{2 E_i E_j (1 - \cos \theta_{ij})}{s}, \\ y_{ij}^D &= \frac{2 \min(E_i^2, E_j^2) (1 - \cos \theta_{ij})}{s}, \\ y_{ij}^G &= \frac{8 E_i E_j (1 - \cos \theta_{ij})}{9 (E_i + E_j)^2}, \end{aligned} \quad (2.9)$$

where the factor of 8/9 in the Geneva algorithm is simply to ensure that the maximum value of y_{cut} that reconstructs three jets from three partons is 1/3 as it is for the other two algorithms. When particles combine, there is some ambiguity as to how to add the energies and momenta. In all three schemes, we use the E scheme i.e. we merely add four momenta,

$$p_{ij}^\mu = p_i^\mu + p_j^\mu. \quad (2.10)$$

Other choices such as the E0 or P schemes where the cluster is made massless by rescaling the momentum or energy give similar results.

Of these variables, the D , C , T_{minor} and y_4^D distributions have been studied in [11].

2.2 Structure of Perturbative Prediction

The differential cross-section at centre-of-mass energy \sqrt{s} for one of these four-jet variables (O_4) at next-to-leading order is described by two coefficients, B_{O_4} and C_{O_4} which represent the leading and next-to-leading order perturbative contributions,

$$\frac{1}{\sigma_0} \cdot O_4 \frac{d\sigma}{dO_4} = \left(\frac{\alpha_s(\mu)}{2\pi} \right)^2 B_{O_4} + \left(\frac{\alpha_s(\mu)}{2\pi} \right)^3 \left(2\beta_0 \log \left(\frac{\mu^2}{s} \right) B_{O_4} + C_{O_4} \right). \quad (2.11)$$

Both B_{O_4} and C_{O_4} are scale independent and do not depend on the beam energy. However, the running coupling α_s is calculated at renormalization scale μ which is commonly chosen to be the *physical* scale, $\mu = \sqrt{s}$. Compared to the leading order prediction, which decays monotonically with increasing μ , the next-to-leading order term reduces the scale dependence somewhat through the first coefficient of the beta-function, $\beta_0 = (33 - 2N_f)/6$. For five active quark flavours, $\beta_0 = 3.833$.

The individual coefficients B_{O_4} and C_{O_4} depend on the number of colours and flavours, or equivalently, the group casimirs of the standard model. As such, four jet event shapes may be used to simultaneously constrain the strong interaction gauge group as well as the strong coupling constant.

2.3 Scale choice and theoretical uncertainty

As mentioned above, for hadronic observables in electron-positron annihilation it is common to choose the renormalisation scale to be the physical scale $\mu = \sqrt{s}$. This choice is motivated by naturalness arguments and the fact that choosing a scale far from \sqrt{s} introduces large logarithms of the form $\log(\mu/\sqrt{s})$ in eq. (2.11). Since the renormalisation scale is only a theoretical construct, it has become common practice to estimate the uncertainty engendered by truncating the perturbative expansion by varying μ by factors about the physical scale.

Other approaches have been considered with rather different scale choices. One such approach is to stipulate that the next-to-leading order coefficient vanishes. That is to say that the LO and NLO predictions coincide.² This occurs at the scale,

$$\mu^{FAC} = \sqrt{s} \exp \left(-\frac{C_{O_4}}{4B_{O_4}\beta_0} \right), \quad (2.12)$$

and is called the scale of *fastest apparent convergence* (FAC) [30]. As we will see, C_{O_4} is typically 50-100 times larger than B_{O_4} so that μ^{FAC} may be as small as 10^{-2} – 10^{-3} of the physical scale.

Another common choice is to select the scale where the NLO prediction is most insensitive to the choice of scale [31]. However, this scale is very close to the FAC scale (15% smaller) so

²In other words, the ratio of NLO to LO predictions commonly called the K-factor is identically unity.

that the *Principle of Minimal Sensitivity* scale (PMS) predictions lie very close to the FAC scale prediction.

While even higher order corrections remain uncalculated, varying the renormalisation scale can only give a crude indication of the theoretical uncertainty. Therefore, in an attempt to make a fair estimate of the theoretical uncertainty on the NLO prediction we will show both the physical scale and FAC scale predictions.

2.4 Infrared behaviour

Four jet event shapes typically depend on the event having some volume and not lying entirely in a plane. Typical hadronic events contain more than 20 hadrons and it is extremely unlikely that the value of any event shape is precisely zero for any experimental event. However, in a LO or NLO fixed order parton calculation, there only four or five partons present in the final state and, when one or more are soft, the calculated O_4 may approach zero. In such circumstances, soft gluon singularities cause the fixed order prediction to become wildly unstable and grow logarithmically. In the small O_4 limits, the perturbative coefficients have the following form,

$$\begin{aligned} B_{O_4} &\rightarrow A_{32}L^3 + A_{22}L^2 + A_{12}L + A_{02}, \\ C_{O_4} &\rightarrow A_{53}L^5 + A_{43}L^4 + A_{33}L^3 + A_{23}L^2 + A_{13}L + A_{03}, \end{aligned} \quad (2.13)$$

where $L = \log(1/O_4)$ and A_{nm} are (as yet) undetermined coefficients. Whenever L is sufficiently large, resummation effects will be important.³ In comparing with data, we therefore choose to make a cut on the size of O_4 which is typically in the range 0.001 — 0.01, since for such small values of O_4 we do not trust the NLO prediction. In comparing with the DELPHI data, this cut will usually be the lower edge of the second data bin.

³Whether the coefficients exponentiate and can be resummed will depend on the observable.

3 Comparison with existing results

3.1 Four jet rates

As a check of the numerical results, Table 1 shows the predictions for each of the three Monte Carlo programs for the four jet rate for three jet clustering algorithms; the Jade-E0, Durham-E [28], and Geneva-E [29] algorithms. We show results with $\alpha_s(M_Z) = 0.118$ for three values of the jet resolution parameter y_{cut} . There is good agreement with the results from the other two calculations.

Algorithm	y_{cut}	MENLO PARC	DEBRECEN	EERAD2
Durham	0.005	$(1.04 \pm 0.02) \cdot 10^{-1}$	$(1.05 \pm 0.01) \cdot 10^{-1}$	$(1.05 \pm 0.01) \cdot 10^{-1}$
	0.01	$(4.70 \pm 0.06) \cdot 10^{-2}$	$(4.66 \pm 0.02) \cdot 10^{-2}$	$(4.65 \pm 0.02) \cdot 10^{-2}$
	0.03	$(6.82 \pm 0.08) \cdot 10^{-3}$	$(6.87 \pm 0.04) \cdot 10^{-3}$	$(6.86 \pm 0.03) \cdot 10^{-3}$
Geneva	0.02	$(2.56 \pm 0.06) \cdot 10^{-1}$	$(2.63 \pm 0.06) \cdot 10^{-1}$	$(2.61 \pm 0.05) \cdot 10^{-1}$
	0.03	$(1.71 \pm 0.03) \cdot 10^{-1}$	$(1.75 \pm 0.03) \cdot 10^{-1}$	$(1.72 \pm 0.03) \cdot 10^{-1}$
	0.05	$(8.58 \pm 0.15) \cdot 10^{-2}$	$(8.37 \pm 0.12) \cdot 10^{-2}$	$(8.50 \pm 0.06) \cdot 10^{-2}$
JADE-E0	0.005	$(3.79 \pm 0.08) \cdot 10^{-1}$	$(3.88 \pm 0.07) \cdot 10^{-1}$	$(3.87 \pm 0.03) \cdot 10^{-1}$
	0.01	$(1.88 \pm 0.03) \cdot 10^{-1}$	$(1.92 \pm 0.01) \cdot 10^{-1}$	$(1.93 \pm 0.01) \cdot 10^{-1}$
	0.03	$(3.46 \pm 0.05) \cdot 10^{-2}$	$(3.37 \pm 0.01) \cdot 10^{-2}$	$(3.35 \pm 0.01) \cdot 10^{-2}$

Table 1: The four-jet fraction as calculated by MENLO PARC, DEBRECEN and EERAD2, for the different jet recombination schemes and varying y_{cut} . The rate is normalized by the $\mathcal{O}(\alpha_s)$ total hadronic cross-section, $\sigma_{\text{had}} = \sigma_0 (1 + \alpha_s/\pi)$.

3.2 Shape variables

As mentioned earlier, Nagy and Trócsányi [11] have computed C_D with their Monte Carlo DEBRECEN. In Table 2 we show the leading and next-to-leading order coefficients B_D and C_D calculated by EERAD2, together with the DEBRECEN result. The two calculations are clearly consistent with one another, with the quoted errors overlapping in almost all cases. The errors from EERAD2 are of the order of 2% in each bin, except in the tail of the distribution where the errors rise as high as 10%. The infrared enhancement of the distribution described in section 2.4 means that the Monte Carlo procedure favours the phase space region corresponding to small values of the D parameter, so that the large D tail suffers larger errors. In fact C_D drops by four orders of magnitude over the kinematic range of the observable so it is necessary to use importance sampling with respect to the observable distribution to ensure sufficient Monte Carlo points are produced in the high D region. This is also true for all of the other shape variables.

In addition, Nagy and Trócsányi have also presented results for the next-to-leading order

coefficients for thrust minor T_{minor} and the jet transition variable in the Durham scheme y_4^D [11]. Although we do not present a detailed comparison here, we note that the agreement is qualitatively the same as discussed for the D parameter above. We find that the distributions extend beyond the range of coefficients presented in [11], with non-zero coefficients for bins in the ranges $0.5 < T_{\text{minor}} < 0.58$ and $0.125 < y_4^D < 0.17$.

D	B_D	C_D	DEBRECEN
0.0200	$(3.79 \pm 0.01) \cdot 10^2$	$(1.47 \pm 0.00) \cdot 10^4$	$(1.08 \pm 0.06) \cdot 10^4$
0.0600	$(2.32 \pm 0.01) \cdot 10^2$	$(1.25 \pm 0.01) \cdot 10^4$	$(1.24 \pm 0.02) \cdot 10^4$
0.1000	$(1.45 \pm 0.01) \cdot 10^2$	$(8.69 \pm 0.04) \cdot 10^3$	$(8.59 \pm 0.12) \cdot 10^3$
0.1400	$(1.04 \pm 0.01) \cdot 10^2$	$(6.39 \pm 0.03) \cdot 10^3$	$(6.24 \pm 0.12) \cdot 10^3$
0.1800	$(7.68 \pm 0.04) \cdot 10^1$	$(4.89 \pm 0.03) \cdot 10^3$	$(4.99 \pm 0.11) \cdot 10^3$
0.2200	$(5.87 \pm 0.03) \cdot 10^1$	$(3.88 \pm 0.03) \cdot 10^3$	$(3.85 \pm 0.06) \cdot 10^3$
0.2600	$(4.66 \pm 0.07) \cdot 10^1$	$(3.04 \pm 0.03) \cdot 10^3$	$(2.98 \pm 0.05) \cdot 10^3$
0.3000	$(3.75 \pm 0.07) \cdot 10^1$	$(2.51 \pm 0.04) \cdot 10^3$	$(2.52 \pm 0.05) \cdot 10^3$
0.3400	$(3.07 \pm 0.05) \cdot 10^1$	$(2.02 \pm 0.03) \cdot 10^3$	$(1.94 \pm 0.05) \cdot 10^3$
0.3800	$(2.41 \pm 0.03) \cdot 10^1$	$(1.61 \pm 0.03) \cdot 10^3$	$(1.59 \pm 0.04) \cdot 10^3$
0.4200	$(1.97 \pm 0.04) \cdot 10^1$	$(1.37 \pm 0.02) \cdot 10^3$	$(1.37 \pm 0.03) \cdot 10^3$
0.4600	$(1.56 \pm 0.03) \cdot 10^1$	$(1.09 \pm 0.01) \cdot 10^3$	$(1.06 \pm 0.03) \cdot 10^3$
0.5000	$(1.32 \pm 0.01) \cdot 10^1$	$(8.97 \pm 0.14) \cdot 10^2$	$(8.72 \pm 0.19) \cdot 10^2$
0.5400	$(1.05 \pm 0.02) \cdot 10^1$	$(7.12 \pm 0.15) \cdot 10^2$	$(7.11 \pm 0.16) \cdot 10^2$
0.5800	$(8.46 \pm 0.16) \cdot 10^0$	$(5.79 \pm 0.12) \cdot 10^2$	$(5.68 \pm 0.14) \cdot 10^2$
0.6200	$(6.60 \pm 0.16) \cdot 10^0$	$(4.55 \pm 0.09) \cdot 10^2$	$(4.46 \pm 0.21) \cdot 10^2$
0.6600	$(5.32 \pm 0.13) \cdot 10^0$	$(3.58 \pm 0.07) \cdot 10^2$	$(3.52 \pm 0.11) \cdot 10^2$
0.7000	$(3.99 \pm 0.09) \cdot 10^0$	$(2.80 \pm 0.09) \cdot 10^2$	$(2.74 \pm 0.09) \cdot 10^2$
0.7400	$(3.06 \pm 0.05) \cdot 10^0$	$(2.05 \pm 0.08) \cdot 10^2$	$(2.08 \pm 0.08) \cdot 10^2$
0.7800	$(2.26 \pm 0.04) \cdot 10^0$	$(1.58 \pm 0.04) \cdot 10^2$	$(1.54 \pm 0.06) \cdot 10^2$
0.8200	$(1.54 \pm 0.04) \cdot 10^0$	$(1.05 \pm 0.03) \cdot 10^2$	$(1.03 \pm 0.04) \cdot 10^2$
0.8600	$(9.72 \pm 0.21) \cdot 10^{-1}$	$(6.72 \pm 0.29) \cdot 10^1$	$(6.66 \pm 0.31) \cdot 10^1$
0.9000	$(5.63 \pm 0.16) \cdot 10^{-1}$	$(3.85 \pm 0.17) \cdot 10^1$	$(3.89 \pm 0.20) \cdot 10^1$
0.9400	$(2.62 \pm 0.07) \cdot 10^{-1}$	$(1.71 \pm 0.10) \cdot 10^1$	$(1.71 \pm 0.19) \cdot 10^1$
0.9800	$(5.34 \pm 0.11) \cdot 10^{-2}$	$(3.15 \pm 0.27) \cdot 10^0$	$(2.60 \pm 1.30) \cdot 10^0$

Table 2: The leading and next-to-leading order coefficients for the D parameter. The NLO coefficient predicted by Nagy and Trócsányi Monte Carlo DEBRECEN [11] is also shown.

4 New results

In this section we extend the analysis of 4 jet-like event shape observables already found in the literature by reporting the leading and next-to-leading order coefficients for the light hemisphere mass, the narrow hemisphere broadening, Aplanarity and the jet transition variable in both the JADE and Geneva schemes, y_4^J and y_4^G . In particular, we examine the relative sizes of the two terms by inspecting the K factor (at the physical scale) for each variable across the allowed kinematic range of the distributions.

For all the variables presented in this section, we must be careful to differentiate between the true behaviour of the distribution as the observable tends to zero and the behaviour in fixed order perturbation theory. Each of the observables should have a smooth behaviour as $O_4 \rightarrow 0$ rather than the divergent behaviour exhibited by the coefficients according to equation 2.13. To recover a smooth result in this limit it is necessary to resum powers of $\log(1/O_4)$ where possible, a procedure which has been performed already for many 3 jet-like variables [32, 25]

4.1 Light Hemisphere Mass

M_L^2/s	$B_{M_L^2/s}$	$C_{M_L^2/s}$
0.0150	$(3.23 \pm 0.08) \cdot 10^2$	$(1.41 \pm 0.01) \cdot 10^4$
0.0250	$(1.88 \pm 0.02) \cdot 10^2$	$(8.85 \pm 0.10) \cdot 10^3$
0.0350	$(1.25 \pm 0.02) \cdot 10^2$	$(5.97 \pm 0.11) \cdot 10^3$
0.0450	$(8.52 \pm 0.10) \cdot 10^1$	$(4.14 \pm 0.08) \cdot 10^3$
0.0550	$(5.97 \pm 0.06) \cdot 10^1$	$(3.04 \pm 0.04) \cdot 10^3$
0.0650	$(4.20 \pm 0.09) \cdot 10^1$	$(2.15 \pm 0.05) \cdot 10^3$
0.0750	$(3.02 \pm 0.07) \cdot 10^1$	$(1.58 \pm 0.05) \cdot 10^3$
0.0850	$(2.13 \pm 0.03) \cdot 10^1$	$(1.11 \pm 0.02) \cdot 10^3$
0.0950	$(1.39 \pm 0.04) \cdot 10^1$	$(7.66 \pm 0.23) \cdot 10^2$
0.1050	$(8.75 \pm 0.20) \cdot 10^0$	$(4.97 \pm 0.17) \cdot 10^2$
0.1150	$(5.18 \pm 0.13) \cdot 10^0$	$(3.27 \pm 0.07) \cdot 10^2$
0.1250	$(2.59 \pm 0.12) \cdot 10^0$	$(1.66 \pm 0.07) \cdot 10^2$
0.1350	$(8.97 \pm 0.35) \cdot 10^{-1}$	$(6.61 \pm 0.41) \cdot 10^1$
0.1450	$(2.49 \pm 0.13) \cdot 10^{-1}$	$(1.79 \pm 0.09) \cdot 10^1$
0.1550	$(5.00 \pm 0.27) \cdot 10^{-2}$	$(3.75 \pm 0.26) \cdot 10^0$
0.1650	$(1.46 \pm 0.21) \cdot 10^{-3}$	$(2.30 \pm 0.37) \cdot 10^{-1}$

Table 3: The leading and next-to-leading order coefficients for the light jet mass M_L^2/s .

As defined before, the light hemisphere mass is the smaller invariant mass of the two hemispheres formed by separating the event by a plane normal to the thrust axis. The NLO coefficient $C_{M_L^2/s}$ evaluated at the physical scale $\mu = \sqrt{s}$ together with the LO term is given

in Table 3. The errors are estimates from the numerical program and are typically 2-3% for each entry. As with the previously known results on four jet event shapes, the NLO terms are significantly larger than the LO term. Here, we see that $C_{M_L^2/s}$ is typically 50 times larger than $B_{M_L^2/s}$ so that even when the additional factor of $\alpha_s/2\pi$ is restored, the NLO correction is large. This is illustrated in Fig. 1 where the K factor defined by,

$$K_{O_4} = 1 + \left(\frac{\alpha_s(\sqrt{s})}{2\pi} \right) \frac{C_{O_4}}{B_{O_4}}, \quad (4.1)$$

is shown for $O_4 = M_L^2/s$. We see that the K factor increases with the value of the observable, rising from 1.8 at small M_L^2/s up to 2.4. This behaviour is similar to that observed for other four jet event shapes [11].

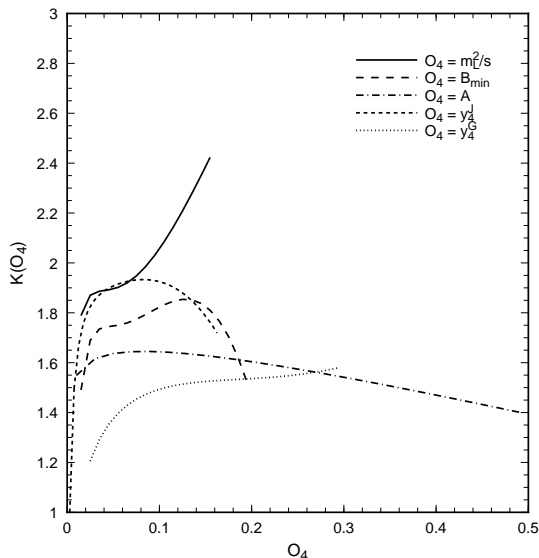


Figure 1: The K-factors defined according to eq. (4.1) for four jet event shapes, the light hemisphere mass (solid), narrow jet broadening (long-dashed), Aplanarity (dot-dashed) and jet transition variables in the JADE (short-dashed) and Geneva (dotted) schemes. Each variable has a different kinematic range.

4.2 Narrow Hemisphere Broadening

Narrow hemisphere broadening, B_{\min} , is defined in a similar manner to the light hemisphere mass. The event is again divided into two hemispheres by the plane normal to the thrust axis, but now the momenta transverse to the thrust axis is summed (normalised by the sum of absolute momenta) in each hemisphere. The narrow hemisphere is that with the least transverse momentum with respect to the thrust axis. Numerical results for this variable as calculated by EERAD2 can be found in Table 4. As with the light hemisphere mass, the

NLO contribution is significant yielding a K factor of roughly 1.7 over most of the kinematic range of the variable (see Fig. 1).

B_{\min}	$B_{B_{\min}}$	$C_{B_{\min}}$
0.0150	$(1.19 \pm 0.01) \cdot 10^3$	$(3.41 \pm 0.07) \cdot 10^4$
0.0250	$(7.04 \pm 0.06) \cdot 10^2$	$(2.56 \pm 0.02) \cdot 10^4$
0.0350	$(4.80 \pm 0.02) \cdot 10^2$	$(1.92 \pm 0.04) \cdot 10^4$
0.0450	$(3.39 \pm 0.02) \cdot 10^2$	$(1.41 \pm 0.02) \cdot 10^4$
0.0550	$(2.49 \pm 0.02) \cdot 10^2$	$(1.07 \pm 0.02) \cdot 10^4$
0.0650	$(1.89 \pm 0.02) \cdot 10^2$	$(8.04 \pm 0.12) \cdot 10^3$
0.0750	$(1.43 \pm 0.02) \cdot 10^2$	$(6.29 \pm 0.12) \cdot 10^3$
0.0850	$(1.08 \pm 0.01) \cdot 10^2$	$(4.81 \pm 0.08) \cdot 10^3$
0.0950	$(8.19 \pm 0.04) \cdot 10^1$	$(3.65 \pm 0.08) \cdot 10^3$
0.1050	$(6.23 \pm 0.08) \cdot 10^1$	$(2.77 \pm 0.09) \cdot 10^3$
0.1150	$(4.69 \pm 0.06) \cdot 10^1$	$(2.10 \pm 0.04) \cdot 10^3$
0.1250	$(3.37 \pm 0.04) \cdot 10^1$	$(1.45 \pm 0.04) \cdot 10^3$
0.1350	$(2.36 \pm 0.04) \cdot 10^1$	$(1.09 \pm 0.03) \cdot 10^3$
0.1450	$(1.64 \pm 0.03) \cdot 10^1$	$(7.07 \pm 0.25) \cdot 10^2$
0.1550	$(9.82 \pm 0.12) \cdot 10^0$	$(4.48 \pm 0.15) \cdot 10^2$
0.1650	$(5.08 \pm 0.12) \cdot 10^0$	$(2.18 \pm 0.10) \cdot 10^2$
0.1750	$(1.71 \pm 0.04) \cdot 10^0$	$(7.53 \pm 0.33) \cdot 10^1$
0.1850	$(4.32 \pm 0.11) \cdot 10^{-1}$	$(1.59 \pm 0.12) \cdot 10^1$
0.1950	$(5.47 \pm 0.11) \cdot 10^{-2}$	$(1.34 \pm 0.24) \cdot 10^0$

Table 4: The leading and next-to-leading order coefficients for the narrow jet broadening B_{\min} .

4.3 Aplanarity

As described earlier, Aplanarity is essentially the smallest eigenvalue of the quadratic momentum tensor. The NLO coefficient C_A evaluated at the physical scale $\mu = \sqrt{s}$ together with the LO term is given in Table 5. Once again, the NLO terms are significantly larger than the LO term B_A and, as can be seen in Fig. 1 gives rise to K factor of roughly 1.5.

4.4 Jet transition variables

As previously stated the jet transition variable y_4^S describes the scale where two jets merge, thereby changing a four jet event into a three jet event. This is essentially the same as the derivative of the four jet rate with respect to the jet resolution parameter y_{cut} . However, the number of jets in an event is dependent on the jet finding algorithm used to define the ‘closeness’ of particles which is compared with y_{cut} . In [11] the transition rate for the

A	B_A	C_A
0.0300	$(7.25 \pm 0.04) \cdot 10^1$	$(2.48 \pm 0.10) \cdot 10^3$
0.0500	$(3.87 \pm 0.03) \cdot 10^1$	$(1.40 \pm 0.07) \cdot 10^3$
0.0700	$(2.35 \pm 0.02) \cdot 10^1$	$(7.65 \pm 0.58) \cdot 10^2$
0.0900	$(1.57 \pm 0.02) \cdot 10^1$	$(5.55 \pm 0.40) \cdot 10^2$
0.1100	$(1.06 \pm 0.01) \cdot 10^1$	$(4.07 \pm 0.36) \cdot 10^2$
0.1300	$(7.45 \pm 0.12) \cdot 10^0$	$(2.34 \pm 0.34) \cdot 10^2$
0.1500	$(5.19 \pm 0.07) \cdot 10^0$	$(1.75 \pm 0.20) \cdot 10^2$
0.1700	$(3.76 \pm 0.08) \cdot 10^0$	$(1.23 \pm 0.28) \cdot 10^2$
0.1900	$(2.68 \pm 0.04) \cdot 10^0$	$(9.42 \pm 1.25) \cdot 10^1$
0.2100	$(2.02 \pm 0.03) \cdot 10^0$	$(6.37 \pm 0.98) \cdot 10^1$
0.2300	$(1.32 \pm 0.02) \cdot 10^0$	$(4.19 \pm 0.99) \cdot 10^1$
0.2500	$(9.70 \pm 0.16) \cdot 10^{-1}$	$(3.14 \pm 0.67) \cdot 10^1$
0.2700	$(6.43 \pm 0.16) \cdot 10^{-1}$	$(2.08 \pm 0.45) \cdot 10^1$
0.2900	$(4.28 \pm 0.14) \cdot 10^{-1}$	$(1.25 \pm 0.34) \cdot 10^1$
0.3100	$(2.87 \pm 0.12) \cdot 10^{-1}$	$(7.58 \pm 1.36) \cdot 10^0$
0.3300	$(1.79 \pm 0.03) \cdot 10^{-1}$	$(6.13 \pm 1.67) \cdot 10^0$
0.3500	$(1.07 \pm 0.02) \cdot 10^{-1}$	$(3.94 \pm 0.91) \cdot 10^0$
0.3700	$(6.66 \pm 0.20) \cdot 10^{-2}$	$(2.00 \pm 0.40) \cdot 10^0$
0.3900	$(3.30 \pm 0.20) \cdot 10^{-2}$	$(9.26 \pm 3.71) \cdot 10^{-1}$
0.4100	$(1.56 \pm 0.09) \cdot 10^{-2}$	$(4.00 \pm 1.52) \cdot 10^{-1}$
0.4300	$(5.58 \pm 0.22) \cdot 10^{-3}$	$(1.50 \pm 0.92) \cdot 10^{-1}$
0.4500	$(1.53 \pm 0.18) \cdot 10^{-3}$	$(7.44 \pm 3.27) \cdot 10^{-2}$
0.4700	$(1.80 \pm 0.23) \cdot 10^{-4}$	$(1.76 \pm 7.87) \cdot 10^{-3}$
0.4900	$(1.38 \pm 0.45) \cdot 10^{-5}$	$(9.93 \pm 54.90) \cdot 10^{-5}$

Table 5: The leading and next-to-leading order coefficients for Aplanarity.

the Durham jet finding algorithm [28] is given and we have checked that our results are consistent with these predictions. Here, we provide results for two other jet algorithms, the JADE and Geneva [29] schemes for which the jet finding measures are given in eq. (2.9). We note that the Geneva algorithm enjoys the same benefits as the Durham algorithm in that it is also supposed to exponentiate, enabling infrared logarithms to be safely resummed. It also ensures that softly radiated gluons are clustered with hard partons unless the angle of separation between two soft gluons is much smaller than the angular separation between them and a hard parton.

Our results for the two schemes are given in Tables 6 and 7. As can be seen from the tables the NLO coefficients are large, which is again reflected in the large corrections shown in Fig. 1. The K factor for the JADE scheme is roughly 1.8-1.9, but is slightly smaller for the Geneva algorithm, typically in the region 1.4-1.6.

y_4^G	$B_{y_4^G}$	$C_{y_4^G}$
0.0250	$(8.00 \pm 0.04) \cdot 10^2$	$(9.93 \pm 0.34) \cdot 10^3$
0.0350	$(5.59 \pm 0.04) \cdot 10^2$	$(9.91 \pm 0.30) \cdot 10^3$
0.0450	$(4.15 \pm 0.03) \cdot 10^2$	$(8.57 \pm 0.13) \cdot 10^3$
0.0550	$(3.15 \pm 0.03) \cdot 10^2$	$(7.31 \pm 0.18) \cdot 10^3$
0.0650	$(2.47 \pm 0.02) \cdot 10^2$	$(5.96 \pm 0.12) \cdot 10^3$
0.0750	$(1.93 \pm 0.02) \cdot 10^2$	$(4.99 \pm 0.14) \cdot 10^3$
0.0850	$(1.50 \pm 0.02) \cdot 10^2$	$(3.96 \pm 0.11) \cdot 10^3$
0.0950	$(1.23 \pm 0.01) \cdot 10^2$	$(3.36 \pm 0.13) \cdot 10^3$
0.1050	$(9.88 \pm 0.12) \cdot 10^1$	$(2.84 \pm 0.06) \cdot 10^3$
0.1150	$(7.90 \pm 0.09) \cdot 10^1$	$(2.19 \pm 0.09) \cdot 10^3$
0.1250	$(6.07 \pm 0.08) \cdot 10^1$	$(1.69 \pm 0.11) \cdot 10^3$
0.1350	$(4.79 \pm 0.07) \cdot 10^1$	$(1.53 \pm 0.08) \cdot 10^3$
0.1450	$(3.84 \pm 0.06) \cdot 10^1$	$(1.15 \pm 0.04) \cdot 10^3$
0.1550	$(3.00 \pm 0.05) \cdot 10^1$	$(8.41 \pm 0.53) \cdot 10^2$
0.1650	$(2.26 \pm 0.04) \cdot 10^1$	$(6.52 \pm 0.36) \cdot 10^2$
0.1750	$(1.61 \pm 0.02) \cdot 10^1$	$(4.99 \pm 0.33) \cdot 10^2$
0.1850	$(1.21 \pm 0.02) \cdot 10^1$	$(3.60 \pm 0.23) \cdot 10^2$
0.1950	$(8.71 \pm 0.27) \cdot 10^0$	$(2.53 \pm 0.20) \cdot 10^2$
0.2050	$(5.70 \pm 0.16) \cdot 10^0$	$(1.78 \pm 0.17) \cdot 10^2$
0.2150	$(3.89 \pm 0.09) \cdot 10^0$	$(1.20 \pm 0.11) \cdot 10^2$
0.2250	$(2.41 \pm 0.06) \cdot 10^0$	$(6.83 \pm 0.87) \cdot 10^1$
0.2350	$(1.43 \pm 0.05) \cdot 10^0$	$(4.87 \pm 0.36) \cdot 10^1$
0.2450	$(7.69 \pm 0.30) \cdot 10^{-1}$	$(2.57 \pm 0.25) \cdot 10^1$
0.2550	$(3.78 \pm 0.09) \cdot 10^{-1}$	$(1.18 \pm 0.13) \cdot 10^1$
0.2650	$(1.50 \pm 0.04) \cdot 10^{-1}$	$(4.57 \pm 0.79) \cdot 10^0$
0.2750	$(4.20 \pm 0.17) \cdot 10^{-2}$	$(1.15 \pm 0.35) \cdot 10^0$
0.2850	$(4.59 \pm 0.39) \cdot 10^{-3}$	$(1.16 \pm 0.65) \cdot 10^{-1}$
0.2950	$(5.37 \pm 0.91) \cdot 10^{-5}$	$(2.15 \pm 1.11) \cdot 10^{-3}$

Table 6: The leading and next-to-leading order coefficients for the jet transition variable in the Geneva-E algorithm y_4^G .

y_4^J	$B_{y_4^J}$	$C_{y_4^J}$
0.0075	$(6.02 \pm 0.01) \cdot 10^2$	$(1.75 \pm 0.01) \cdot 10^4$
0.0125	$(3.60 \pm 0.01) \cdot 10^2$	$(1.33 \pm 0.02) \cdot 10^4$
0.0175	$(2.47 \pm 0.01) \cdot 10^2$	$(1.02 \pm 0.04) \cdot 10^4$
0.0225	$(1.78 \pm 0.01) \cdot 10^2$	$(7.63 \pm 0.32) \cdot 10^3$
0.0275	$(1.34 \pm 0.01) \cdot 10^2$	$(6.19 \pm 0.16) \cdot 10^3$
0.0325	$(1.01 \pm 0.01) \cdot 10^2$	$(4.76 \pm 0.12) \cdot 10^3$
0.0375	$(7.88 \pm 0.08) \cdot 10^1$	$(3.86 \pm 0.11) \cdot 10^3$
0.0425	$(6.19 \pm 0.05) \cdot 10^1$	$(3.07 \pm 0.16) \cdot 10^3$
0.0475	$(4.99 \pm 0.05) \cdot 10^1$	$(2.38 \pm 0.12) \cdot 10^3$
0.0525	$(3.89 \pm 0.05) \cdot 10^1$	$(2.08 \pm 0.11) \cdot 10^3$
0.0575	$(3.13 \pm 0.05) \cdot 10^1$	$(1.54 \pm 0.05) \cdot 10^3$
0.0625	$(2.43 \pm 0.04) \cdot 10^1$	$(1.26 \pm 0.03) \cdot 10^3$
0.0675	$(1.90 \pm 0.03) \cdot 10^1$	$(9.68 \pm 0.58) \cdot 10^2$
0.0725	$(1.49 \pm 0.04) \cdot 10^1$	$(7.70 \pm 0.35) \cdot 10^2$
0.0775	$(1.21 \pm 0.02) \cdot 10^1$	$(5.89 \pm 0.41) \cdot 10^2$
0.0825	$(9.38 \pm 0.18) \cdot 10^0$	$(4.83 \pm 0.35) \cdot 10^2$
0.0875	$(6.94 \pm 0.09) \cdot 10^0$	$(3.50 \pm 0.19) \cdot 10^2$
0.0925	$(5.36 \pm 0.11) \cdot 10^0$	$(2.48 \pm 0.27) \cdot 10^2$
0.0975	$(3.85 \pm 0.06) \cdot 10^0$	$(1.93 \pm 0.19) \cdot 10^2$
0.1025	$(2.84 \pm 0.07) \cdot 10^0$	$(1.26 \pm 0.11) \cdot 10^2$
0.1075	$(1.97 \pm 0.07) \cdot 10^0$	$(9.99 \pm 1.22) \cdot 10^1$
0.1125	$(1.30 \pm 0.06) \cdot 10^0$	$(6.69 \pm 0.94) \cdot 10^1$
0.1175	$(8.32 \pm 0.37) \cdot 10^{-1}$	$(3.57 \pm 0.52) \cdot 10^1$
0.1225	$(4.94 \pm 0.07) \cdot 10^{-1}$	$(2.36 \pm 0.44) \cdot 10^1$
0.1275	$(3.05 \pm 0.10) \cdot 10^{-1}$	$(1.85 \pm 0.38) \cdot 10^1$
0.1325	$(1.70 \pm 0.03) \cdot 10^{-1}$	$(8.38 \pm 3.15) \cdot 10^0$
0.1375	$(8.94 \pm 0.29) \cdot 10^{-2}$	$(4.99 \pm 1.15) \cdot 10^0$
0.1425	$(4.20 \pm 0.12) \cdot 10^{-2}$	$(2.01 \pm 0.38) \cdot 10^0$
0.1475	$(1.67 \pm 0.07) \cdot 10^{-2}$	$(1.08 \pm 0.73) \cdot 10^0$
0.1525	$(5.51 \pm 0.44) \cdot 10^{-3}$	$(3.94 \pm 2.32) \cdot 10^{-1}$
0.1575	$(8.48 \pm 0.58) \cdot 10^{-4}$	$(4.37 \pm 2.44) \cdot 10^{-2}$

Table 7: The leading and next-to-leading order coefficients for the jet transition variable in the JADE-E0 algorithm y_4^J .

5 Comparison with experimental data

Four jet event shape observables have been studied extensively by the four LEP experiments. However, the most complete analysis of event shape variables has been carried out by the DELPHI collaboration [33]. Here, they study all of the event shape variables discussed in section 2. Distributions based on charged particles alone as well as charged and neutral particles are presented. In this section, we wish to examine whether or not these event shapes can be described by fixed order perturbation theory. As discussed earlier, to avoid numerical instabilities in the infrared region where fixed order perturbation theory is no longer valid we impose a cut on the smallness of the variable that is generally equal to the lower edge of the second bin. More precisely, that is,

$$\begin{aligned}
 D &> 0.008, \\
 T_{\text{minor}} &> 0.02, \\
 M_L^2/s &> 0.01, \\
 B_{\text{min}} &> 0.01, \\
 A &> 0.005, \\
 y_4^D &> 0.002, \\
 y_4^J &> 0.002.
 \end{aligned} \tag{5.1}$$

The experimental distributions are normalised to the hadronic cross section (rather than the Born cross section) and are also not weighted by the observable, but are rather,

$$\frac{1}{\sigma_{\text{had}}} \cdot \frac{d\sigma}{dO_4} = \left(\frac{\alpha_s(\mu)}{2\pi} \right)^2 \frac{B_{O_4}}{O_4} + \left(\frac{\alpha_s(\mu)}{2\pi} \right)^3 \left(2\beta_0 \log \left(\frac{\mu^2}{s} \right) \frac{B_{O_4}}{O_4} + \frac{C_{O_4} - 2B_{O_4}}{O_4} \right). \tag{5.2}$$

Throughout, we choose $\alpha_s(M_Z) = 0.118$ which is consistent with the current world average [34]. In each case, the theoretical predictions have been evaluated using bins of the same size as in the experiment and therefore appear as histograms in the plots. The data is corrected for detector effects, but not for hadronisation effects.

Figs. 2, 3 and 4 show the comparison between the leading order and next-to-leading order predictions evaluated at the physical scale $\mu = \sqrt{s} = M_Z$ for narrow jet broadening, light hemisphere mass and Aplanarity with the published DELPHI data [33]. We see that in all three cases, the LO prediction undershoots the data by a significant factor (about a factor of four), and that including the NLO correction improves the situation but still gives a rate that is much lower than the data. However, the NLO prediction still contains a large renormalisation scale uncertainty. Usually, one varies the choice of scale about the physical scale by a factor of two or so, but as discussed earlier, the FAC scale defined in eq. (2.12) is an attractive alternative choice in that the known ultraviolet logarithms are resummed [35]. For both of these variables, the FAC scale is significantly less than the physical scale, for example, for B_{min} , $\mu^{\text{FAC}} \sim 0.06\sqrt{s}$. This has the effect of increasing α_s , thereby increasing the NLO prediction and in both cases, we see much improved agreement at larger values of the observable. At smaller values, and particularly in the region where the data turns over

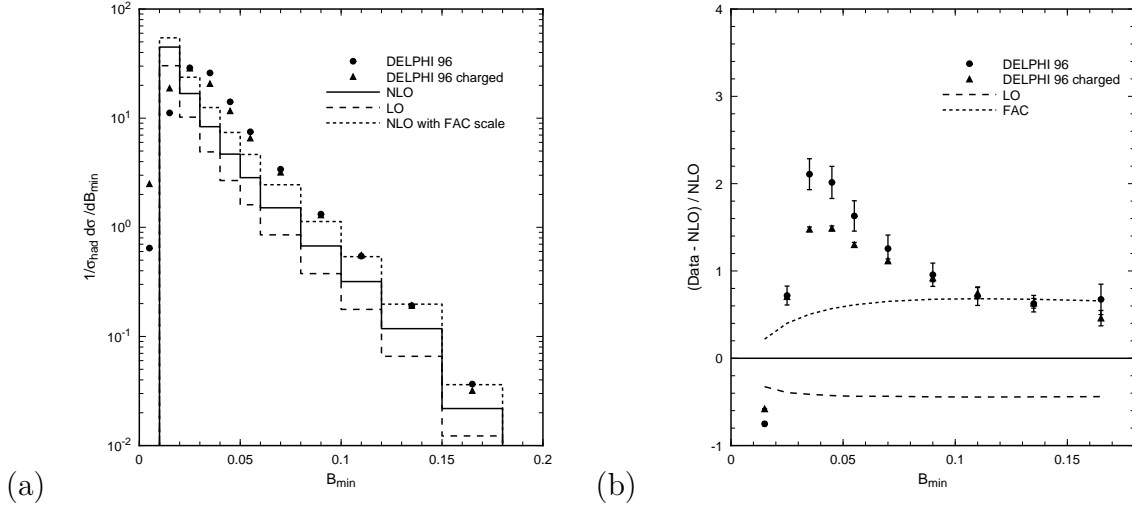


Figure 2: The leading order (dashed) and next-to-leading order (solid) predictions evaluated at the physical scale $\mu = \sqrt{s} = M_Z$ for (a) $1/\sigma_{\text{had}} \cdot d\sigma/dB_{\text{min}}$ compared to the published DELPHI data [33] and (b) the difference between data and NLO theory (normalised to NLO). The short-dashed line shows the next-to-leading order prediction using the FAC scale (see eq. (2.12)).

the agreement is still poor. This, of course, is where the infrared logarithms are large and need to be resummed. Furthermore, we also expect non-perturbative hadronisation effects or power corrections to influence the perturbative shape of the distribution we have been concerned with [36, 37]. These contributions (together with resummation of the infrared logarithms) have played an important role in extracting useful information from analyses of three jet shape variables, and are likely to be important in analysing four jet event shapes.

A similar comparison of the perturbative predictions for the jet transition rates with the DELPHI measurements⁴ is made in Figs. 5 and 6. Once again, the LO distribution lies well below the data. This time, the NLO prediction lies much closer to the data for most of the available kinematic range. The FAC scale rate usually lies above the NLO prediction so that the data lies within the range of uncertainty engendered by the renormalisation group.

For completeness, Figs. 7 and 8 show the DELPHI data and perturbative predictions for the D parameter and T_{minor} respectively. As expected from the analysis of Nagy and Trócsányi [11], the LO prediction for D is too low by a factor of about four, while at the physical scale $\mu = \sqrt{s} = M_Z$ the NLO distribution is roughly twice as large but still lies a factor of two below the data. However, for the FAC scale (which for the D parameter is approximately $0.035\sqrt{s}$) the prediction overshoots by 50% or so for $D > 0.1$ where the fixed order prediction is least affected by large infrared logs.

⁴The DELPHI data gives the differential jet rate rather than the jet transition variable. Up to a small (\sim few %) correction from five (and more) jet events falling into a four jet configuration, the two quantities coincide at fixed order.

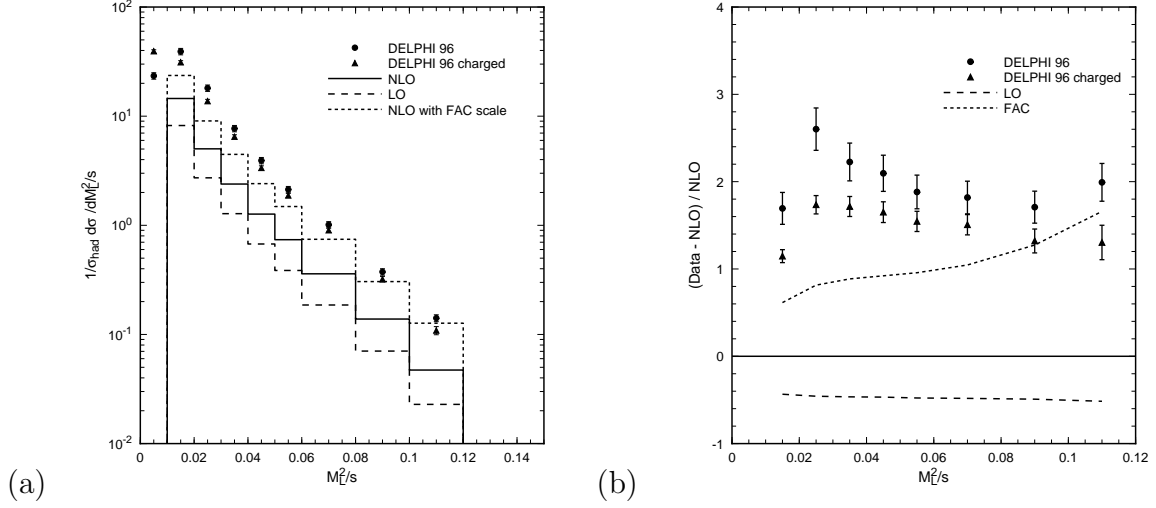


Figure 3: The leading order (dashed) and next-to-leading order (solid) predictions evaluated at the physical scale $\mu = \sqrt{s} = M_Z$ for (a) $1/\sigma_{\text{had}} \cdot d\sigma/d(M_L^2/s)$ compared to the published DELPHI data [33] and (b) the difference between data and NLO theory (normalised to NLO). The short-dashed line shows the next-to-leading order prediction using the FAC scale (see eq. (2.12)).

The importance of resumming these logs is clearly shown in Fig. 8 where the T_{minor} distribution is shown. For $T_{\text{minor}} > 0.1$ the data again lies between the next-to-leading order predictions at the physical and FAC scales (which encompass an uncertainty of about a factor of almost three for $T_{\text{minor}} \sim 0.2$). However, the turn-over at $T_{\text{minor}} = 0.1$ cannot be modelled without resumming the large logs which cause the perturbative prediction to grow rapidly. The same is true at small values of the light hemisphere mass and narrow jet broadening although there the effects are less pronounced because of the choice of bin sizes.

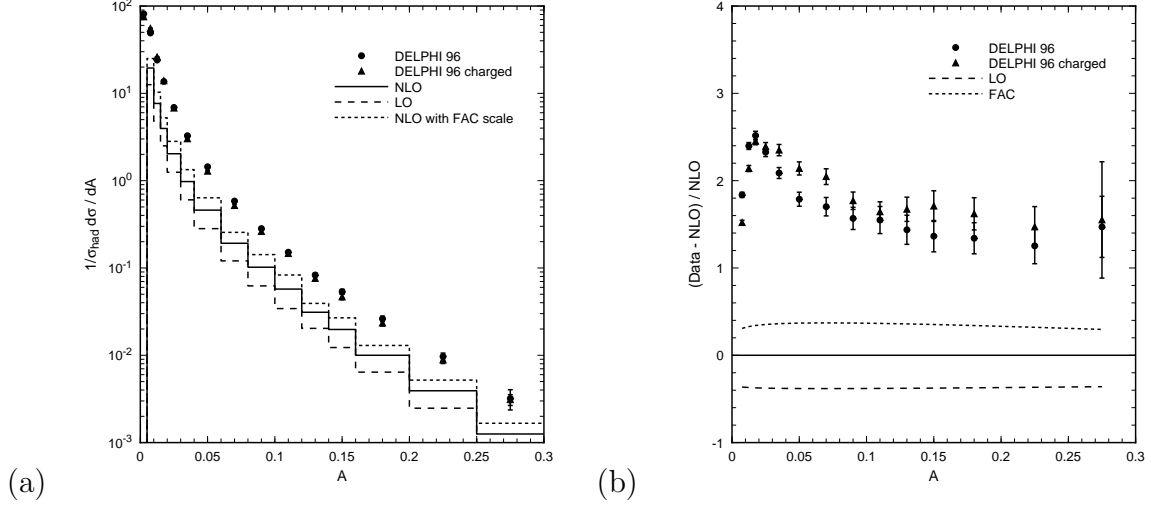


Figure 4: The leading order (dashed) and next-to-leading order (solid) predictions evaluated at the physical scale $\mu = \sqrt{s} = M_Z$ for (a) $1/\sigma_{\text{had}} \cdot d\sigma/dA$ compared to the published DELPHI data [33] and (b) the difference between data and NLO theory (normalised to NLO). The short-dashed line shows the next-to-leading order prediction using the FAC scale (see eq. (2.12)).

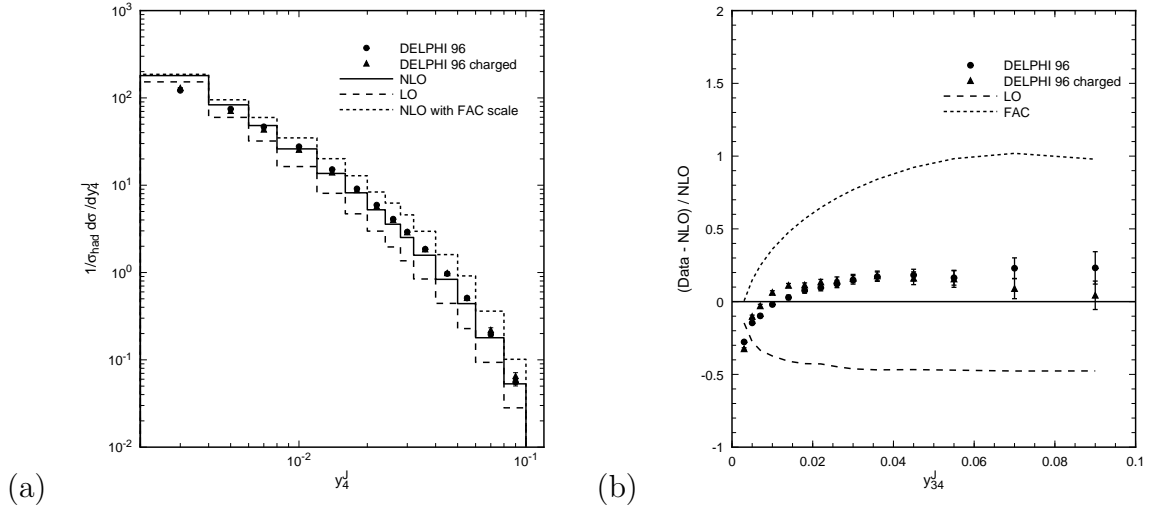


Figure 5: The leading order (dashed) and next-to-leading order (solid) predictions evaluated at the physical scale $\mu = \sqrt{s} = M_Z$ for (a) $1/\sigma_{\text{had}} \cdot d\sigma/dy_4^J$ compared to the published DELPHI data [33] and (b) the difference between data and NLO theory (normalised to NLO). The short-dashed line shows the next-to-leading order prediction using the FAC scale (see eq. (2.12)).

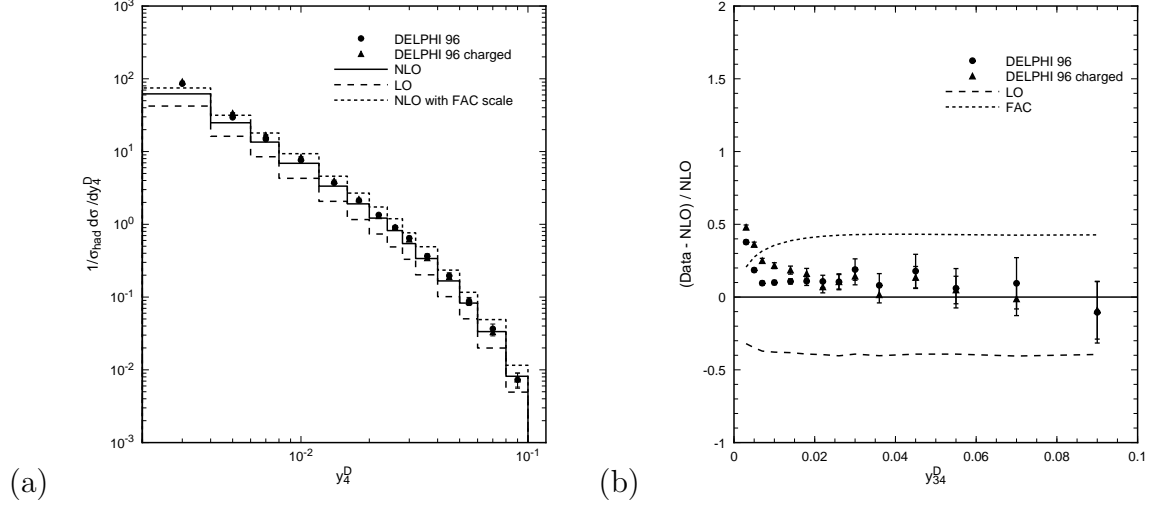


Figure 6: The leading order (dashed) and next-to-leading order (solid) predictions evaluated at the physical scale $\mu = \sqrt{s} = M_Z$ for (a) $1/\sigma_{\text{had}} \cdot d\sigma/dy_4^D$ compared to the published DELPHI data [33] and (b) the difference between data and NLO theory (normalised to NLO). The short-dashed line shows the next-to-leading order prediction using the FAC scale (see eq. (2.12)).

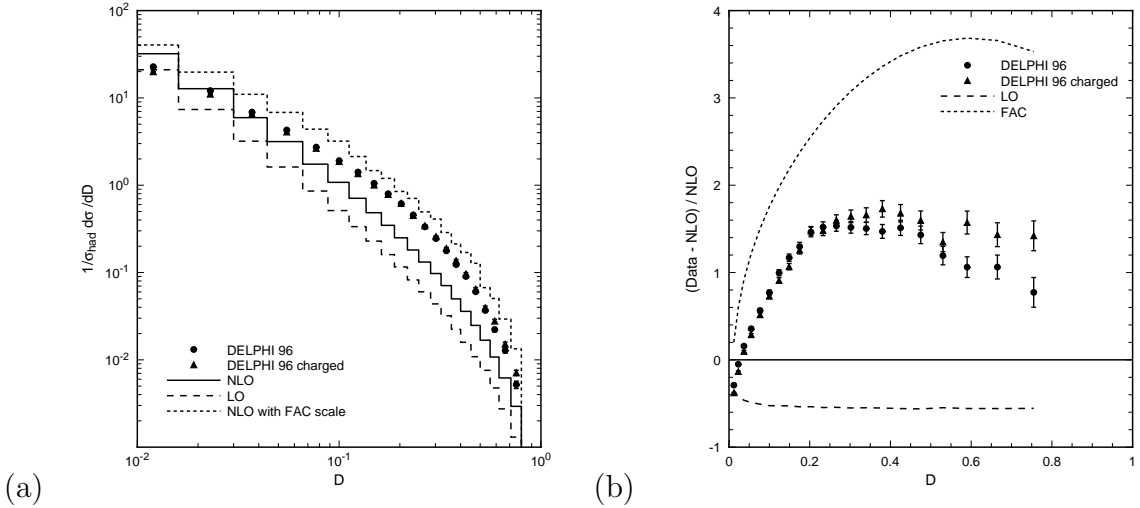


Figure 7: The leading order (dashed) and next-to-leading order (solid) predictions evaluated at the physical scale $\mu = \sqrt{s} = M_Z$ for (a) $1/\sigma_{\text{had}} \cdot d\sigma/dD$ compared to the published DELPHI data [33] and (b) the difference between data and NLO theory (normalised to NLO). The short-dashed line shows the next-to-leading order prediction using the FAC scale (see eq. (2.12)).

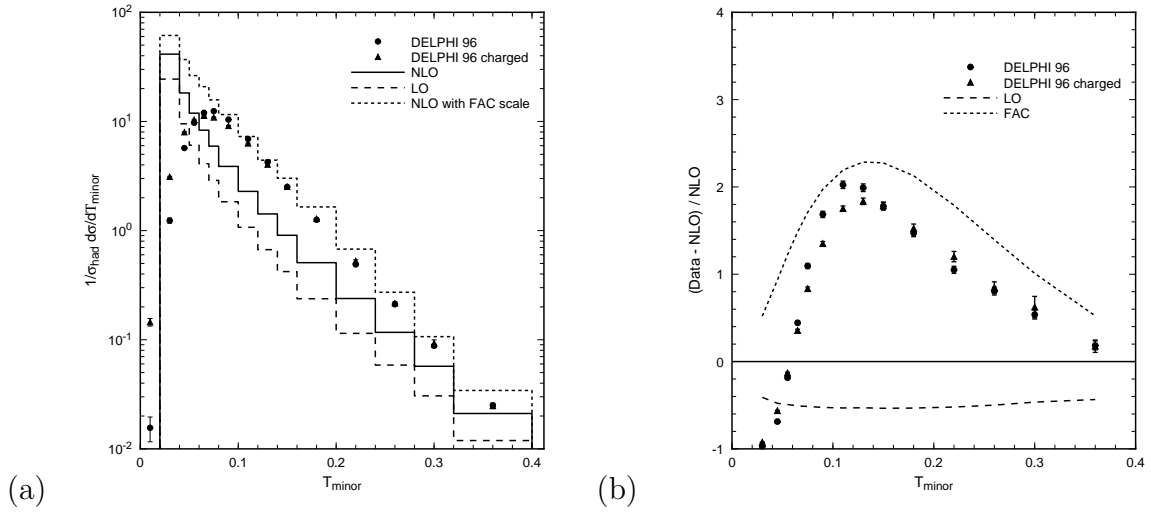


Figure 8: The leading order (dashed) and next-to-leading order (solid) predictions evaluated at the physical scale $\mu = \sqrt{s} = M_Z$ for (a) $1/\sigma_{\text{had}} \cdot d\sigma/dT_{\text{minor}}$ compared to the published DELPHI data [33] and (b) the difference between data and NLO theory (normalised to NLO). The short-dashed line shows the next-to-leading order prediction using the FAC scale (see eq. (2.12)).

6 Conclusions

In this paper we have introduced a new Monte Carlo program for the calculation of 4 jet like observables in electron-positron annihilation. This program, **EERAD2**, is based on the known squared matrix elements for $\gamma^* \rightarrow 4$ and 5 partons and numerically implements the necessary cancellations between the different final states using a hybrid of the commonly used subtraction and slicing schemes. This infrared cancellation scheme is detailed in the appendix.

We have checked that the numerical results obtained with **EERAD2** are consistent with the two other available four jet programs **MENLO**, **PARC** and **DEBRECEN** by recalculating the distributions for some of the previously determined four jet event variables (such as the D parameter, thrust minor and the jet transition rate for the Durham jet algorithm) as well as the four jet rate. Within the (estimated) statistical Monte Carlo errors, there is excellent agreement.

We have also presented the leading and next-to-leading order scale independent coefficients for some previously uncalculated observables; the light hemisphere mass, narrow jet broadening, Aplanarity and the four jet transition variables with respect to the JADE and Geneva jet finding algorithms. For each of these observables, the next-to-leading order corrections calculated at the physical scale significantly increase the rate compared to leading order (see fig. 1). The renormalisation scale dependence is also rather large.

Furthermore, for each of these observables, we have made a comparison with the published data collected at LEP 1 energies by the DELPHI collaboration. With the exception of the y_4 distributions, the data lies well above the NLO prediction, apart from in the infrared region where the NLO prediction grows rapidly (and where resummation of large logarithms is essential). Using the FAC scale, which is of the order of 0.1–1% of the physical scale, increases the predicted rate and in general produces a slightly better agreement with the data. Taking together the size of the NLO corrections, the renormalisation scale dependence and poor agreement with data it appears that the inclusion of even higher order corrections and/or power corrections will be necessary to extract any useful information from these observations.

Although at first sight this may seem discouraging, it is instructive to compare this situation with the well-established results for the 3 jet-like variable 1 – Thrust. In this case, the next-to-leading order coefficient is also large compared to the leading order term, resulting in a K factor at the physical scale which varies from 1.4–1.6 throughout most of the kinematic range of the variable. These values are very similar to the case for the four jet observables that we have already discussed. In addition, it is also possible to compare the pure perturbative prediction for 1 – Thrust with the DELPHI data, as we have done for the four jet variables in section 4. This yields results which are qualitatively very similar to those shown for the D -parameter and T_{minor} in Figs. 7 and 8. In these cases, it is clear that the perturbative prediction – either at the physical scale or using the FAC choice – is insufficient to describe the data. However, after resummation of large logarithms and the

inclusion of non-perturbative power corrections proportional to the inverse of the energy scale of the process, $1/Q$, it is known that the data for $1 - \text{Thrust}$ can be described very well [37]. In fact the thrust distribution forms a text-book example of how to interpret hadronic final states within QCD.

From this we conclude that discarding four jet-like event shape variables as unreliable at next-to-leading order is premature without proper consideration of the types of non-perturbative terms that have been successfully included for a variety of three jet-like observables. In this we disagree with the conclusions of reference [11].

In addition to these correction terms, all of the distributions that we have considered exhibit the infrared logarithmic behaviour (as the observable tends to zero) that is inevitable in a fixed order calculation. These logarithms are present in the coefficients B_{O_4} and C_{O_4} and can be parametrized in the form shown in eq. (2.13). By performing a fit to the distributions at low enough values of the variable O_4 one should be able to extract the values of the coefficients A_{nm} and, where possible, perform exponentiation to resum the infrared logarithms.

Acknowledgements

We thank Walter Giele for useful and stimulating discussions. We also thank Siggie Bethke for pointing out that the JADE-E0 jet algorithm does not use the E0 recombination scheme. JMC and MC thank the UK Particle Physics and Astronomy Research Council for research studentships. EWNG thanks the theory groups at CERN and Fermilab for their kind hospitality during the early stages of this work. This work was supported in part by the EU Fourth Framework Programme ‘Training and Mobility of Researchers’, Network ‘Quantum Chromodynamics and the Deep Structure of Elementary Particles’, contract FMRX-CT98-0194 (DG-12 - MIHT).

A Cancellation of infrared singularities

In order to compute next-to-leading order quantities in perturbation theory, it is necessary to combine the contribution from n -parton one-loop Feynman diagrams with the $(n + 1)$ -parton bremsstrahlung process. The virtual matrix elements are divergent and contain both infrared and ultraviolet singularities. The ultraviolet poles are removed by renormalisation, however the soft and collinear infrared poles are only cancelled when the virtual graphs are combined with the bremsstrahlung process. Although the cancellation of infrared poles can be done analytically for simple processes, for complicated processes, it is necessary to resort to numerical techniques.

A.1 A simple example

The numerical problem has been nicely formulated by Kunszt and Soper [38] by means of a simple example integral,

$$\mathcal{I} = \lim_{\epsilon \rightarrow 0} \left\{ \int_0^1 \frac{dx}{x} x^\epsilon F(x) - \frac{1}{\epsilon} F(0) \right\}, \quad (\text{A.1})$$

where $F(x)$ is a known but complicated function representing the $(n + 1)$ -parton bremsstrahlung matrix elements. Here x represents the angle between two partons or the energy of a gluon and the integral over x represents the additional phase space of the extra parton. As $x \rightarrow 0$, the integrand is regularised by the x^ϵ factor as in dimensional regularisation, however, the first term is still divergent as $\epsilon \rightarrow 0$. This divergence is cancelled by the second term - the n -parton one-loop contribution - so that the integral is finite. A variety of methods to compute \mathcal{I} have been developed.

The method used by Ellis, Ross and Terrano [1] is also known as the subtraction method. Here, a divergent term is subtracted from the first term and added to the second,

$$\begin{aligned} \mathcal{I} &= \lim_{\epsilon \rightarrow 0} \left\{ \int_0^1 \frac{dx}{x} x^\epsilon (F(x) - F(0)) + F(0) \int_0^1 \frac{dx}{x} x^\epsilon - \frac{1}{\epsilon} F(0) \right\} \\ &= \int_0^1 \frac{dx}{x} (F(x) - F(0)), \end{aligned} \quad (\text{A.2})$$

so that the integral is manifestly finite. This method has the advantages of requiring (in principle) no extra theoretical cutoffs and making no approximations. However, in practice, there are still large cancellations in the numerator and there is a hidden parameter which cuts the integral off at the lower end. Recently, this technique has been developed to describe general processes [16].

An alternate approach known as the phase space slicing method has also been widely used [2]. The integration region is divided into two parts, $0 < x < \delta$ and $\delta < x < 1$. In the first region, the function $F(x)$ can be approximated by $F(0)$ provided the arbitrary cutoff

$\delta \ll 1$,

$$\begin{aligned}\mathcal{I} &\sim \lim_{\epsilon \rightarrow 0} \left\{ \int_{\delta}^1 \frac{dx}{x} x^{\epsilon} F(x) + F(0) \int_0^{\delta} \frac{dx}{x} x^{\epsilon} - \frac{1}{\epsilon} F(0) \right\} \\ &\sim \int_{\delta}^1 \frac{dx}{x} F(x) + F(0) \ln(\delta).\end{aligned}\tag{A.3}$$

This method is extremely portable [18] since the soft and collinear approximations of the matrix elements and phase space are universal. This makes it easy to apply to a wide variety of physically interesting processes. However, the disadvantage is the presence of the arbitrary cutoff δ . The integral should not depend on δ , and the δ dependence of the two terms in eq. (A.3) should cancel. Since the approximations are reliable only when δ is small, this can give rise to numerical problems.

Finally, we can imagine combinations of these two approaches - the hybrid approach. There are two scales in the problem, δ and Δ . In the region $0 < x < \delta$, we adopt the slicing procedure, while in the range $\delta < x < \Delta$ we add and subtract an analytically integrable set of universal terms, $E(x)$, to eq. (A.3),

$$\mathcal{I} \sim \int_{\delta}^1 \frac{dx}{x} F(x) + F(0) \ln(\delta) - \int_{\delta}^{\Delta} \frac{dx}{x} E(x) + \int_{\delta}^{\Delta} \frac{dx}{x} E(x),\tag{A.4}$$

which on rearrangement yields,

$$\mathcal{I} \sim \int_{\delta}^1 \frac{dx}{x} (F(x) - E(x)\Theta(\Delta - x)) + \int_{\delta}^{\Delta} \frac{dx}{x} E(x) + F(0) \ln(\delta).\tag{A.5}$$

Because we explicitly add and subtract the same quantity, there can be no dependence on Δ which can therefore be taken to be large. However, the slicing approximation requires $\delta \rightarrow 0$. For this approach to be useful, two conditions must be satisfied. First, the second term in eq. (A.5) must be evaluated analytically without making any approximation in the phase space and should produce a term $-F(0) \ln(\delta)$ from the lower boundary that explicitly cancels the third (slicing) term. This allows the limit $\delta \rightarrow 0$ to be taken (inasmuch as that can be achieved numerically). Second, $F(x) \sim E(x)$ as $x \rightarrow 0$ and more usefully $E(x)$ is smooth and as close to $F(x)$ as possible over the whole range of $x < \Delta$, so that the first term in eq. (A.5) can be safely evaluated numerically. This is the technique we have adopted in this paper.

A.2 Singular behaviour of Matrix Elements

Clearly the choice of the subtraction function $E(x)$ requires some care, as does the integration over the phase space variables x . To help us do this in a sensible way, we first recall the well known singular behaviour of the matrix elements. This is most clearly seen by decomposing the amplitude according to the various colour structures. For example, in the process,

$$e^+e^- \rightarrow q\bar{q} + n\ g,$$

the amplitude can be written as,

$$\mathcal{M}(Q_1, \overline{Q}_2; 1, \dots, n) = \hat{\mathcal{S}}_\mu^{n+2}(Q_1; 1, \dots, n; \overline{Q}_2) V^\mu, \quad (\text{A.6})$$

where the hadronic current is given by,

$$\hat{\mathcal{S}}_\mu^{n+2}(Q_1; 1, \dots, n; \overline{Q}_2) = i e g^n \sum_{P(1, \dots, n)} (T^{a_1} \dots T^{a_n})_{c_1 c_2} S_\mu(Q_1; 1, \dots, n; \overline{Q}_2). \quad (\text{A.7})$$

Here, $\mathcal{S}_\mu(Q_1; 1, \dots, n; \overline{Q}_2)$ represents the colourless subamplitude where the gluons (with colours a_1, \dots, a_n) are emitted in an ordered way from the quarks (with colours c_1 and c_2). The colour matrices are normalised such that,

$$\text{Tr}(T^{a_i} T^{a_j}) = \frac{1}{2} \delta^{a_i a_j}.$$

By summing over all permutations of gluon emission, all Feynman diagrams and colour structures are accounted for. On squaring, we find that for $n \geq 1$ the leading colour piece is simply,

$$|\hat{\mathcal{S}}_\mu^{n+2} V^\mu|^2 = e^2 \left(\frac{g^2 N}{2} \right)^n \left(\frac{N^2 - 1}{N} \right) \sum_{P(1, \dots, n)} \left(|\mathcal{S}_\mu(Q_1; 1, \dots, n; \overline{Q}_2) V^\mu|^2 + \mathcal{O}\left(\frac{1}{N^2}\right) \right). \quad (\text{A.8})$$

The subleading terms are slightly more complicated, but may be straightforwardly obtained by considering diagrams with gluons replaced by one or more photons.⁵

The advantage of the colour decomposition is that the ordered subamplitudes have particularly simple singular limits. For example, in the limit where gluon u is soft, we have the QED-like factorisation into an eikonal factor multiplied by the colour ordered amplitude with gluon u removed, but the ordering of the hard gluons preserved,

$$\begin{aligned} & \left| \mathcal{S}_\mu(Q_1; 1, \dots, a, u, b, \dots, n; \overline{Q}_2) V^\mu \right|^2 \\ & \rightarrow S_{aub}(s_{ab}, s_{au}, s_{ub}) \left| \mathcal{S}_\mu(Q_1; 1, \dots, a, b, \dots, n; \overline{Q}_2) V^\mu \right|^2, \end{aligned} \quad (\text{A.9})$$

with the eikonal factor given by,

$$S_{aub}(s_{ab}, s_{au}, s_{ub}) = \frac{4s_{ab}}{s_{au}s_{ub}}. \quad (\text{A.10})$$

Similarly, in the limit where two particles become collinear, the sub-amplitudes factorise. For example, if gluons a and b become collinear and form gluon c , then only colour connected gluons give a singular contribution. For example,

$$\left| \mathcal{S}_\mu(Q_1; 1, \dots, a, b, \dots, n; \overline{Q}_2) V^\mu \right|^2 \rightarrow P_{gg \rightarrow g}(z, s_{ab}) \left| \mathcal{S}_\mu(Q_1; 1, \dots, c, \dots, n; \overline{Q}_2) V^\mu \right|^2. \quad (\text{A.11})$$

⁵Here, we have focussed on the two quark process, however, the same type of colour decomposition can be applied to the four quark process, $e^+ e^- \rightarrow q \bar{q} Q \bar{Q} + (n-2)g$, (see for example Ref. [39, 40]). The structure appears to be more complicated, however the singular behaviour of individual contributions follows the same pattern.

For gluons that are not colour connected, there is no singular contribution as $s_{ab} \rightarrow 0$, and, when integrated over the small region of phase space where the collinear approximation is valid, give a negligible contribution to the cross section. Here z is the fraction of the momentum carried by one of the gluons and, after integrating over the azimuthal angle of the plane containing the collinear particles with respect to the rest of the hard process, the collinear splitting function $P_{gg \rightarrow g}$ is given by,

$$P_{gg \rightarrow g}(z, s) = \frac{2}{s} P_{gg \rightarrow g}(z) \quad (\text{A.12})$$

where the usual Altarelli-Parisi splitting kernel with the colour factor removed is given by [41],

$$P_{gg \rightarrow g}(z) = \left(\frac{1 + z^4 + (1 - z)^4}{z(1 - z)} \right). \quad (\text{A.13})$$

Similar splitting kernels exist for other combinations of collinear partons [41],

$$P_{qg \rightarrow q}(z) = \left(\frac{1 + z^2}{1 - z} \right), \quad (\text{A.14})$$

$$P_{q\bar{q} \rightarrow g}(z) = \left(z^2 + (1 - z)^2 \right), \quad (\text{A.15})$$

with $P_{gq \rightarrow q}(z) = P_{qg \rightarrow q}(1 - z)$. As before, the colour factors have been removed and azimuthal averaging of the collinear particle plane is understood.

In both the soft and collinear limits, the colour ordered squared amplitudes factorise into a squared amplitude containing one less parton multiplied by a factor that depends on the the unresolved particle and the two adjacent ‘hard’ particles. We view the two ‘hard’ particles as an *antenna* from which the unresolved parton is radiated. It therefore makes sense to divide the phase space in a similar way and to treat the subtraction term as the singular factor for the whole antenna integrated over the unresolved phase space.

A.3 Phase space factorisation

Let us consider an $(n + 1)$ particle phase space described by momenta p_i with $p_i^2 = 0$ for $i = 1, \dots, n$. If the total centre of mass energy is Q , then let us denote the phase space by, $dPS(Q^2; p_1, \dots, p_n)$. As discussed above, we wish to relate the full $(n + 1)$ particle phase space to an n particle phase space whenever one of the original $(n + 1)$ particles is unresolved. Let the unresolved particle be labelled by u and the two adjacent hard particles by a and b , then the phase space can be factorised as,

$$dPS(Q^2; p_1, \dots, p_n) = dPS(Q^2; p_1, \dots, p_{aub}, \dots, p_n) \frac{ds_{aub}}{2\pi} dPS(s_{aub}; p_a, p_u, p_b), \quad (\text{A.16})$$

where $p_{aub} = p_a + p_u + p_b$ and $p_{aub}^2 = s_{aub}$. To factorise the phase space into an n particle phase space multiplied by a factor containing integrals over the unresolved invariants s_{au}

and s_{ub} that appear in the singular limits of the matrix elements, we multiply the r.h.s. of eq. (A.16) by,

$$dPS(s_{AB}; p_A, p_B) / \int dPS(s_{AB}; p_A, p_B), \quad (\text{A.17})$$

where particles A and B have momenta p_A and p_B such that, $p_{aub} = p_{AB} = p_A + p_B$, $p_A^2 = p_B^2 = 0$ and $s_{aub} = s_{AB}$. In other words,

$$\begin{aligned} dPS(Q^2; p_1, \dots, p_n) &= dPS(Q^2; p_1, \dots, p_{AB}, \dots, p_n) \frac{ds_{AB}}{2\pi} dPS(s_{AB}; p_A, p_B) \times dPS^{\text{sing}} \\ &= dPS(Q^2; p_1, \dots, p_A, p_B, \dots, p_n) \times dPS^{\text{sing}}. \end{aligned} \quad (\text{A.18})$$

As desired, we have the phase space for an final state containing n lightlike particles multiplied by dPS^{sing} . Working in four-dimensions and after integration over the Euler angles,

$$\begin{aligned} dPS^{\text{sing}} &= \frac{dPS(s_{aub}; p_a, p_u, p_b)}{\int dPS(s_{AB}; p_A, p_B)} \\ &= \frac{1}{16\pi^2} s_{aub} dx_{au} dx_{ub} dx_{ab} \delta(1 - x_{au} - x_{ub} - x_{ab}), \end{aligned} \quad (\text{A.19})$$

where $x_{ij} = s_{ij}/s_{aub}$. For this to work, a mapping must exist that determines p_A and p_B for a given set of momenta p_a , p_b and p_u . Many choices are possible [17, 42] and we choose the symmetric mapping of [42],

$$\begin{aligned} p_A &= \frac{1}{2} \left[1 + \rho + \frac{s_{ub}(1 + \rho - 2r_1)}{s_{ab} + s_{au}} \right] p_a + r_1 p_u + \frac{1}{2} \left[1 - \rho + \frac{s_{au}(1 - \rho - 2r_1)}{s_{ab} + s_{ub}} \right] p_b, \\ p_B &= \frac{1}{2} \left[1 - \rho - \frac{s_{ub}(1 + \rho - 2r_1)}{s_{ab} + s_{au}} \right] p_a + (1 - r_1) p_u + \frac{1}{2} \left[1 + \rho - \frac{s_{au}(1 - \rho - 2r_1)}{s_{ab} + s_{ub}} \right] p_b, \end{aligned} \quad (\text{A.20})$$

where,

$$r_1 = \frac{s_{ub}}{s_{au} + s_{ub}}, \quad (\text{A.21})$$

and,

$$\rho = \sqrt{\frac{s_{ab}^2 + (s_{au} + s_{ub})s_{ab} + 4r_1(1 - r_1)s_{au}s_{ub}}{s_{ab}s_{aub}}}. \quad (\text{A.22})$$

Note that this transformation approaches the singular limits smoothly. For example, as $s_{au} \rightarrow 0$, then $r_1 \rightarrow 1$, $\rho \rightarrow 1$ and $p_A \rightarrow p_a + p_u$, $p_B \rightarrow p_b$.

A.4 Antenna factorisation of the Matrix elements

Having factorised the phase space, we now wish to find the analogues of the subtraction functions $E(x)$ discussed in Appendix A.1. These functions should ideally be valid over the whole of the antenna phase space dPS^{sing} and, in the soft and collinear regions must match

onto the singular limits discussed in Appendix A.2. In other words, for a given $(n + 1)$ particle amplitude, in the limit where particle u is unresolved,

$$\left| \mathcal{S}_\mu(\dots, a, u, b, \dots) V^\mu \right|^2 \rightarrow \mathcal{A}_{aub} \left| \mathcal{S}_\mu(\dots, A, B, \dots) V^\mu \right|^2, \quad (\text{A.23})$$

where we have replaced the antenna comprising a, u, b by the hard partons A and B to obtain an n particle amplitude. The antenna function \mathcal{A}_{aub} depends on the momenta of the radiated particles a, b and u , but the n particle amplitude $|\mathcal{S}_\mu V^\mu|^2$ does not.

The leading colour contribution to an observable cross section from an $(n + 1)$ particle final state with a particular colour ordering is proportional to,

$$\left(\frac{N^2 - 1}{N^2} \right) \left(\frac{g^2 N}{2} \right)^{n+1} \left| \mathcal{S}_\mu(\dots, a, u, b, \dots) V^\mu \right|^2 \mathcal{J}_{(n+1)} \text{d}PS(Q^2; \dots, p_a, p_u, p_b, \dots), \quad (\text{A.24})$$

where the observable function $\mathcal{J}_{(n+1)}$ represents the cuts applied to the $(n + 1)$ particle phase space to define the observable. Using the factorisation of the matrix elements defined in eq. (A.23), when particle u is unresolved we should subtract,

$$\left(\frac{g^2 N}{2} \right)^{n+1} \mathcal{A}_{aub} \left| \mathcal{S}_\mu(\dots, A, B, \dots) V^\mu \right|^2 \mathcal{J}_{(n)} \text{d}PS(Q^2; \dots, p_a, p_u, p_b, \dots), \quad (\text{A.25})$$

from the $(n + 1)$ particle contribution and, using the phase space factorisation of eq. (A.18), add,

$$\left(\frac{g^2 N}{2} \right)^{n+1} \mathcal{A}_{aub} \text{d}PS^{\text{sing}} \left| \mathcal{S}_\mu(\dots, A, B, \dots) V^\mu \right|^2 \mathcal{J}_{(n)} \text{d}PS(Q^2; \dots, p_A, p_B, \dots), \quad (\text{A.26})$$

to the n particle contribution where both the observable function \mathcal{J} and matrix elements $|\mathcal{S}_\mu V^\mu|^2$ depend only on the momenta of the n remaining hard partons. Note that for any infrared safe observable, in the limit that one particle is unresolved, $\mathcal{J}_{(n+1)} \rightarrow \mathcal{J}_{(n)}$. In the subtraction term eq. (A.25), we use the transformations of eq. (A.20) to map the momenta p_a, p_u and p_b defined in the $(n + 1)$ particle phase space onto the momenta p_A and p_B used in the n -particle matrix elements and observable functions. In eq. (A.26), all dependence on the momenta of particles a, b and u may be integrated out to give the antenna factor, \mathcal{F} ,

$$\mathcal{F}_{AB}(s_{AB}) = \left(\frac{g^2 N}{2} \right) \int \mathcal{A}_{aub} \text{d}PS^{\text{sing}}, \quad (\text{A.27})$$

multiplying the n particle cross section (for a given colour ordered amplitude),

$$\left(\frac{g^2 N}{2} \right)^n \left| \mathcal{S}_\mu(\dots, A, B, \dots) V^\mu \right|^2 \mathcal{J}_{(n)} \text{d}PS(Q^2; \dots, p_A, p_B, \dots). \quad (\text{A.28})$$

The full set of subtraction terms is obtained by summing over all possible antennae.

The Dalitz plot for the $(AB) \rightarrow aub$ phase space is shown in Fig. 9. In the hybrid scheme we are implementing, we use the slicing method of [18] in the region $\min(s_{au}, s_{ub}) < \delta$, and

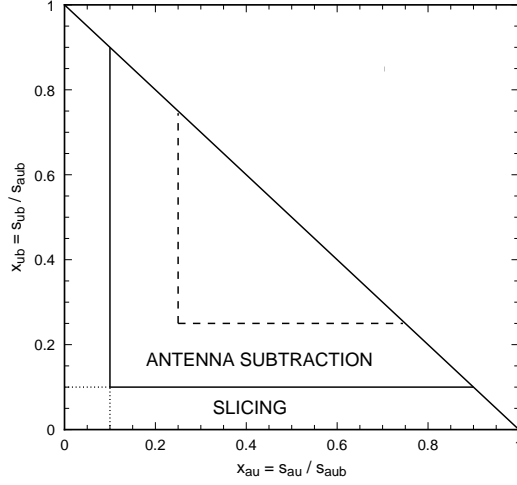


Figure 9: The phase space for the decay $(AB) \rightarrow aub$. The cut $\min(s_{au}, s_{ub}) = \delta$ with $\delta = 0.1 s_{aub}$ is shown as a solid line while $\min(s_{au}, s_{ub}) = \Delta$ is shown as a dashed line for $\Delta = 0.25 s_{aub}$. The region $\min(s_{au}, s_{ub}) < \delta$ defines where the slicing approach is utilised, with the soft and collinear regions demarked by dotted lines. Antenna subtraction is applied when $\delta < \min(s_{au}, s_{ub}) < \Delta$.

the subtraction scheme in the region, $\delta < \min(s_{au}, s_{ub}) < \Delta$. In the slicing region, the phase space and soft and collinear approximations to the matrix elements are kept in $D = 4 - 2\epsilon$ dimensions to regularise the singularities present when either invariant vanishes. Using the approach of [18], there are three separate contributions (a) soft gluon when $\max(s_{au}, s_{ub}) < \delta$, (b) a and u collinear when $s_{au} < \delta$ but $s_{ub} > \delta$ and (c) b and u collinear when $s_{ub} < \delta$ but $s_{au} > \delta$.

Before turning to the explicit forms for the antenna subtraction terms, we note that while quarks are only directly colour connected to one particle - a gluon or antiquark, gluons are directly connected to two particles - the gluon (or quark) on either side. Therefore, while the quark (or antiquark) appear in a single antenna, gluons appear in two. This gives an ambiguity in how to assign the collinear singularities of a pair of gluons to each antenna. Later we will exploit this ambiguity to make the antenna functions \mathcal{A}_{aub} for different pairs of hard partons finite simpler.

A.4.1 Quark-Antiquark antenna

Let us first consider a system containing a quark, antiquark and a gluon. This is produced by an antenna comprising of a hard quark and antiquark pair that decays by radiating a gluon. Any function that has the correct soft gluon and collinear quark/gluon singularities in the appropriate limit is satisfactory. Here the hard particles in the antenna are Q and \bar{Q}

which radiate to form q , \bar{q} and the gluon g . A suitable choice for the antenna function is,

$$\begin{aligned}\mathcal{A}_{qg\bar{q}} &= \frac{|\mathcal{S}_\mu(q; g; \bar{q})V^\mu|^2}{|\mathcal{S}_\mu(Q; \bar{Q})V^\mu|^2} \\ &= \frac{2}{s_{aub}} \left(\frac{x_{au}}{x_{ub}} + \frac{x_{ub}}{x_{au}} + \frac{2x_{ab}x_{aub}}{x_{au}x_{ub}} \right).\end{aligned}\quad (\text{A.29})$$

Because this is proportional to the three parton matrix elements, $|\mathcal{S}_\mu(q; g; \bar{q})V^\mu|^2$, it automatically contains the correct soft and collinear limits. Furthermore, it is smooth over the whole three particle phase space and singularities only appear in the $s_{au} \rightarrow 0$ and $s_{ub} \rightarrow 0$ limits.

Explicitly integrating over the antenna phase space for $\delta < \min(s_{au}, s_{ub}) < \Delta$ we find,

$$\begin{aligned}\mathcal{F}_{Q\bar{Q}}(s_{Q\bar{Q}}) &= \left(\frac{g^2 N}{2} \right) \int \mathcal{A}_{qg\bar{q}} \, dP S^{\text{sing}} \\ &= \left(\frac{\alpha_s N}{2\pi} \right) \left(\ln^2 \left(\frac{\delta}{s_{Q\bar{Q}}} \right) + \frac{3}{2} \ln \left(\frac{\delta}{s_{Q\bar{Q}}} \right) \right) + \mathcal{F}_{Q\bar{Q}}^\Delta \left(\frac{\Delta}{s_{Q\bar{Q}}} \right) + \mathcal{O}(\delta).\end{aligned}\quad (\text{A.30})$$

Since we intend to take the $\delta \rightarrow 0$ limit, the terms of $\mathcal{O}(\delta)$ may be safely neglected. The δ independent function $\mathcal{F}_{Q\bar{Q}}^\Delta$ is given by,

$$\mathcal{F}_{Q\bar{Q}}^\Delta(x) = \left(\frac{\alpha_s N}{2\pi} \right) \left(-\ln^2(x) + \frac{5x}{2} - 2\text{Li}_2(x) + \left(\frac{3}{2} - 2x + \frac{x^2}{2} \right) \ln \left(\frac{1-x}{x} \right) \right). \quad (\text{A.31})$$

A.4.2 Quark-Gluon antenna

For antenna made of a quark Q and gluon G , there are two possible ways of radiating. Either a gluon can be radiated so that a quark-gluon-gluon system is formed, or the gluon may split into a antiquark-quark pair. This latter possibility is subleading in the number of colours and the discussion of situations like this is deferred to sec. A.4.4.

For a quark-gluon-gluon system there is a less obvious choice of antenna function, particularly since the singularity that is produced when the gluon splits sits in more than one antenna. If, in the collinear limit, the gluon splits into an unresolved gluon u which carries momentum fraction z and a hard gluon b with momentum fraction $1-z$, the antenna function should naively be proportional to $P_{gg \rightarrow g}$ which is singular as $z \rightarrow 0$ and $z \rightarrow 1$. This corresponds to singularities as both $s_{ub} \rightarrow 0$ and $s_{ab} \rightarrow 0$. However, because the collinear singularity sits in more than one antenna - the two gluons also occur in a second antenna where the role of the two gluons is reversed - we can make use of the $N = 1$ supersymmetric identity to rewrite $P_{gg \rightarrow g}$ as,

$$P_{gg \rightarrow g} = P_{qg \rightarrow q} + P_{gq \rightarrow q} - P_{q\bar{q} \rightarrow g}. \quad (\text{A.32})$$

The soft singularities as $z \rightarrow 0$ are contained in $P_{gq \rightarrow q}$ while those as $z \rightarrow 1$ are in $P_{qg \rightarrow q}$. We therefore divide $P_{gg \rightarrow g}$ amongst the two antennae such that $P_{gq \rightarrow q}$ sits in the antenna where

gluon u is unresolved. The $z \rightarrow 1$ singularities are placed in the antenna where the role of the two gluons is reversed. The remaining $P_{q\bar{q} \rightarrow g}$ may be divided between the two antennae according to choice. With a slight modification due to the $P_{q\bar{q} \rightarrow g}$ term, the antenna function used for the $Q\bar{Q}$ antenna has the correct limits, so that,

$$\mathcal{A}_{ggg} = \mathcal{A}_{qg\bar{q}} - \frac{2}{s_{aub}} \left(\frac{x_{au}^2}{x_{ub}x_{aub}} \right). \quad (\text{A.33})$$

This is again smooth over the whole three particle phase space with singularities only appearing in the $s_{au} \rightarrow 0$ and $s_{ub} \rightarrow 0$ limits. In particular, as $z \rightarrow 0$, the collinear limit matches onto the soft limit which would not have been the case if we had divided the soft/collinear singularities equally between the two antenna.

After integrating over the antenna phase space for $\delta < \min(s_{au}, s_{ub}) < \Delta$ we find,

$$\begin{aligned} \mathcal{F}_{QG}(s_{QG}) &= \left(\frac{g^2 N}{2} \right) \int \mathcal{A}_{ggg} \, dPS^{\text{sing}} \\ &= \left(\frac{\alpha_s N}{2\pi} \right) \left(\ln^2 \left(\frac{\delta}{s_{QG}} \right) + \frac{10}{6} \ln \left(\frac{\delta}{s_{QG}} \right) \right) + \mathcal{F}_{QG}^\Delta \left(\frac{\Delta}{s_{QG}} \right) \end{aligned} \quad (\text{A.34})$$

with the δ independent function \mathcal{F}_{QG}^Δ is given by,

$$\begin{aligned} \mathcal{F}_{QG}^\Delta(x) &= \left(\frac{\alpha_s N}{2\pi} \right) \left(-\ln^2(x) + \frac{19x}{6} - \frac{x^2}{6} + \frac{x^3}{9} - 2\text{Li}_2(x) \right. \\ &\quad \left. + \left(\frac{10}{6} - 2x + \frac{x^2}{2} - \frac{x^3}{6} \right) \ln \left(\frac{1-x}{x} \right) \right). \end{aligned} \quad (\text{A.35})$$

Antennae containing a gluon and an antiquark are described by,

$$\mathcal{A}_{gg\bar{q}} = \mathcal{A}_{qg\bar{q}}(a \leftrightarrow b), \quad (\text{A.36})$$

and,

$$\mathcal{F}_{G\bar{Q}}(s_{G\bar{Q}}) = \mathcal{F}_{QG}(s_{G\bar{Q}}). \quad (\text{A.37})$$

A.4.3 Gluon-Gluon antenna

For antenna comprising only gluons, we repeat this SUSY inspired trick for each of the resolved gluons so that,

$$\mathcal{A}_{ggg} = \mathcal{A}_{qg\bar{q}} - \frac{2}{s_{aub}} \left(\frac{x_{au}^2}{x_{ub}x_{aub}} + \frac{x_{ub}^2}{x_{au}x_{aub}} \right). \quad (\text{A.38})$$

Note that Kosower [42] has proposed an antenna factorisation for gluonic processes,

$$\mathcal{A}_{ggg}^{\text{Kosower}} = \frac{4}{s_{aub}} \left(\frac{(x_{aub}(x_{aub} - x_{ab}) + x_{ab}^2)^2}{x_{au}x_{ub}x_{ab}x_{sub}} \right), \quad (\text{A.39})$$

which, in the u/b collinear limit regenerates the full $P_{gg \rightarrow g}$ splitting function, as well as the soft limits.

Integration of the antenna function \mathcal{A}_{ggg} over the whole of the subtraction region yields,

$$\begin{aligned}\mathcal{F}_{GG}(s_{GG}) &= \left(\frac{g^2 N}{2}\right) \int \mathcal{A}_{ggg} \, dPS^{\text{sing}} \\ &= \left(\frac{\alpha_s N}{2\pi}\right) \left(\ln^2 \left(\frac{\delta}{s_{GG}} \right) + \frac{11}{6} \ln \left(\frac{\delta}{s_{GG}} \right) \right) + \mathcal{F}_{GG}^\Delta \left(\frac{\Delta}{s_{GG}} \right)\end{aligned}\quad (\text{A.40})$$

with the δ independent function \mathcal{F}_{GG}^Δ is given by,

$$\begin{aligned}\mathcal{F}_{GG}^\Delta(x) &= \left(\frac{\alpha_s N}{2\pi}\right) \left(-\ln^2(x) + \frac{23x}{6} - \frac{2x^2}{6} + \frac{2x^3}{9} - 2\text{Li}_2(x) \right. \\ &\quad \left. + \left(\frac{11}{6} - 2x + \frac{x^2}{2} - \frac{x^3}{3} \right) \ln \left(\frac{1-x}{x} \right) \right).\end{aligned}\quad (\text{A.41})$$

A.4.4 Antenna where a quark-antiquark pair merge

There are also configurations when two (or more) colour lines are present, one ending in an antiquark the other starting with a quark of the same flavour. Here the matrix elements have the form,

$$\left| \mathcal{S}_\mu(\dots, a, \bar{q}|q, b, \dots) V^\mu \right|^2. \quad (\text{A.42})$$

In the collinear limit, the quark-antiquark pinch the two colour lines together to form a single colour line,

$$\left| \mathcal{S}_\mu(\dots, a, \bar{q}|q, b, \dots) V^\mu \right|^2 \rightarrow P_{\bar{q}q \rightarrow g}(z, s_{\bar{q}q}) \left| \mathcal{S}_\mu(\dots, a, G, b, \dots) V^\mu \right|^2, \quad (\text{A.43})$$

with $P_{\bar{q}q \rightarrow G}(z, s)$ given by eqs. (A.12) and (A.15). There is no soft singularity, nor is there any dependence on the type of adjacent parton, a or b . Clearly, the quark-antiquark pair can sit in two antennae, (a, \bar{q}, q) and (\bar{q}, q, b) and we have some freedom of how to assign the singularities to the antennae. There are two obvious choices. Either we divide the singular contribution equally over the two antennae, or, we place the z^2 part of $P_{\bar{q}q \rightarrow g}(z)$ in one antenna and the $(1-z)^2$ part in the other (as we did with the three gluon antenna before). While there appears to be no preference, we follow this latter route so that the antenna function vanishes as the unresolved particle becomes soft,

$$\mathcal{A}_{a\bar{q}q} = \frac{2}{s_{a\bar{q}q}} \left(\frac{x_{a\bar{q}}^2}{x_{\bar{q}q} x_{a\bar{q}q}} \right), \quad (\text{A.44})$$

and,

$$\mathcal{A}_{\bar{q}qb} = \mathcal{A}_{a\bar{q}q}(x_{a\bar{q}} \rightarrow x_{qb}, x_{a\bar{q}q} \leftrightarrow x_{\bar{q}qb}). \quad (\text{A.45})$$

Following this procedure and integrating over the whole of the subtraction region yields,

$$\begin{aligned}\mathcal{F}_{aG}^{N_F}(s_{aG}) &= \left(\frac{g^2 N_F}{2}\right) \int \mathcal{A}_{a\bar{q}q} \, dPS^{\text{sing}} \\ &= \left(\frac{\alpha_s N_F}{2\pi}\right) \left(-\frac{1}{6} \ln\left(\frac{\delta}{s_{aG}}\right)\right) + \mathcal{F}_{aG}^{N_F\Delta}\left(\frac{\Delta}{s_{aG}}\right),\end{aligned}\quad (\text{A.46})$$

and,

$$\mathcal{F}_{Gb}^{N_F}(s_{Gb}) = \mathcal{F}_{aG}^{N_F}(s_{Gb}). \quad (\text{A.47})$$

The factor of N_F arises because each of the N_F quark flavours may contribute. The δ independent function is,

$$\begin{aligned}\mathcal{F}_{aG}^{N_F\Delta}(x) &= \mathcal{F}_{Gb}^{N_F\Delta}(x) \\ &= \left(\frac{\alpha_s N_F}{2\pi}\right) \left(-\frac{2x}{3} + \frac{x^2}{6} - \frac{x^3}{9} - \left(\frac{1}{6} - \frac{x^3}{6}\right) \ln\left(\frac{1-x}{x}\right)\right).\end{aligned}\quad (\text{A.48})$$

A.5 Leading colour contribution to $e^+e^- \rightarrow 4$ jets.

As a pedagogical example, we consider the leading colour contribution relevant for $e^+e^- \rightarrow 4$ jets. The sub-leading pieces are similarly calculated but the resulting expressions are somewhat lengthy due to the many antennae that are involved [40]. At leading order in the number of colours, only the two quark and n gluon process contributes⁶, so, at lowest order, the cross section is given by,

$$\begin{aligned}\frac{d\sigma_4^{\text{LO}}}{\sigma_0} &= \frac{(2\pi)^5}{s} \left(\frac{N^2-1}{N^2}\right) \left(\frac{\alpha_s N}{2\pi}\right)^2 \\ &\times \sum_{P(G_1, G_2)} \left| \mathcal{S}_\mu(Q_1; G_1, G_2; \overline{Q}_2) V^\mu \right|^2 \mathcal{J}_{(4)} \, dPS(Q^2; Q_1 G_1, G_2, \overline{Q}_2) \mathcal{I}_2,\end{aligned}\quad (\text{A.49})$$

where \mathcal{I}_2 is the identical particle factor for the two gluon final state. In practice, the $2!$ permutations precisely cancels the identical particle factor of $1/2!$, and it is more convenient to keep one particular ordering so that,

$$\frac{d\sigma_4^{\text{LO}}}{\sigma_0} = \frac{(2\pi)^5}{s} \left(\frac{N^2-1}{N^2}\right) \left(\frac{\alpha_s N}{2\pi}\right)^2 \left| \mathcal{S}_\mu(Q_1; G_1, G_2; \overline{Q}_2) V^\mu \right|^2 \mathcal{J}_{(4)} \, dPS(Q^2; Q_1 G_1, G_2, \overline{Q}_2). \quad (\text{A.50})$$

Similarly, the leading colour contribution from the five parton bremsstrahlung process is,

$$\frac{d\sigma_5}{\sigma_0} = \frac{(2\pi)^7}{s} \left(\frac{N^2-1}{N^2}\right) \left(\frac{\alpha_s N}{2\pi}\right)^3$$

⁶The four quark process gives a contribution that is suppressed by a factor of N_F/N relative to the leading colour contribution. Numerically this is an important contribution and, together with the other subleading terms, is included in the numerical results presented earlier.

$$\begin{aligned}
& \times \sum_{P(g_1, g_2, g_3)} \left| \mathcal{S}_\mu(q_1; g_1, g_2, g_3; \bar{q}_2) V^\mu \right|^2 \mathcal{J}_{(5)} \, dPS(Q^2; q_1, g_1, g_2, g_3, \bar{q}_2) \mathcal{I}_3, \\
& = \frac{(2\pi)^7}{s} \left(\frac{N^2 - 1}{N^2} \right) \left(\frac{\alpha_s N}{2\pi} \right)^3 \left| \mathcal{S}_\mu(q_1; g_1, g_2, g_3; \bar{q}_2) V^\mu \right|^2 \mathcal{J}_{(5)} \, dPS(Q^2; q_1, g_1, g_2, g_3, \bar{q}_2).
\end{aligned} \tag{A.51}$$

Note that \mathcal{J}_5 projects the five parton momenta onto the four jet like observable. Once again, we can cancel the identical particle factor $\mathcal{I}_3 = 1/3!$ against the $3!$ permutations of the gluons, and retain the single permutation indicated. For this colour ordering, three antennae will contribute, (q_1, g_1, g_2) , (g_1, g_2, g_3) and (g_2, g_3, \bar{q}_2) where in each case the parton in the middle is unresolved. In the first antenna, $\{p_{q_1}, p_{g_1}, p_{g_2}\} \rightarrow \{p_{Q_1}, p_{G_1}\}$ according to eq. (A.20), the slicing cuts are $\min(s_{q_1 g_1}, s_{g_1 g_2}) < \delta$ and the subtraction occurs over the range $\delta < \min(s_{q_1 g_1}, s_{g_1 g_2}) < \Delta$. Similar transformations and cuts act over the other two antenna.

A.5.1 Slicing contribution

For the five parton matrix elements of eq. (A.51), the sum of infrared singularities from the three antennae in the slicing approach gives a contribution to the four particle final state which can be read directly from eq. (3.79) of ref. [18],

$$d\sigma_4^{\text{slice}} = R(Q_1; G_1, G_2; \bar{Q}_2) d\sigma_4^{\text{LO}}. \tag{A.52}$$

Retaining only the leading colour contribution (i.e. dropping the contributions from the four quark process proportional to the number of quark flavours),

$$\begin{aligned}
R(Q_1; G_1, G_2; \bar{Q}_2) &= \left(\frac{\alpha_s N}{2\pi} \right) \frac{1}{\Gamma(1 - \epsilon)} \left[\sum_{ij} \left\{ \frac{1}{\epsilon^2} \left(\frac{4\pi\mu^2}{s_{ij}} \right)^\epsilon - \log^2 \left(\frac{s_{ij}}{\delta} \right) \right\} \right. \\
&\quad \left. + \frac{3}{2\epsilon} \left(\frac{4\pi\mu^2}{\delta} \right)^\epsilon + \frac{197}{18} - \pi^2 \right] \\
&\quad + \left(\frac{\alpha_s}{2\pi} \right) \frac{2b_0}{\epsilon} \frac{1}{\Gamma(1 - \epsilon)} \left(\frac{4\pi\mu^2}{\delta} \right)^\epsilon + \mathcal{O}(\epsilon) + \mathcal{O}(\delta),
\end{aligned}$$

with (at leading order in the number of colours) $b_0 = 11N/6$ and where the sum runs over the pairs of adjacent (colour connected) hard partons, $ij = Q_1 G_1, G_1 G_2$ and $G_2 \bar{Q}_2$.

A.5.2 Subtraction term

Since there are three antennae, we subtract three antennae factors, such that the total subtraction term is,

$$\frac{d\sigma_5^{\text{sub}}}{\sigma_0} = \frac{(2\pi)^7}{s} \left(\frac{N^2 - 1}{N^2} \right) \left(\frac{\alpha_s N}{2\pi} \right)^3 dPS(Q^2; q_1, g_1, g_2, g_3, \bar{q}_2)$$

$$\begin{aligned}
& \times \left(\mathcal{A}_{q_1 g_1 g_2} \left| \mathcal{S}_\mu(Q_1; G_1, g_3; \bar{q}_2) V^\mu \right|^2 \mathcal{J}_{(4)} \right. \\
& \quad + \mathcal{A}_{g_1 g_2 g_3} \left| \mathcal{S}_\mu(q_1; G_1, G_2; \bar{q}_2) V^\mu \right|^2 \mathcal{J}_{(4)} \\
& \quad \left. + \mathcal{A}_{g_2 g_2 \bar{q}_2} \left| \mathcal{S}_\mu(q_1; g_1, G_2; \bar{Q}_2) V^\mu \right|^2 \mathcal{J}_{(4)} \right). \tag{A.53}
\end{aligned}$$

Here, we have used the mappings $\{p_{q_1}, p_{g_1}, p_{g_2}\} \rightarrow \{p_{Q_1}, p_{G_1}\}$ according to eq. (A.20) for the first antenna. We recall that the subtraction occurs over the range $\delta < \min(s_{q_1 g_1}, s_{g_1 g_2}) < \Delta$ and that the observable function \mathcal{J}_4 is applied to the momenta for Q_1, G_1, g_3 and \bar{q}_2 . Similar procedures are applied to the other antennae.

However, we must add these terms back to the four parton contribution. Here it is simplest to re-identify each of the four particle momenta with the momenta relevant for tree level. In other words, for the first antenna, $\{p_{q_1}, p_{g_1}, p_{g_2}\} \rightarrow \{p_{Q_1}, p_{G_1}\}$ as before and $p_{g_3} \rightarrow p_{G_2}, p_{\bar{q}_2} \rightarrow p_{\bar{Q}_2}$. This is safe to do since we integrate over the whole four particle phase space. Altogether, we have,

$$d\sigma_4^{\text{sub}} = \left(\mathcal{F}_{Q_1 G_1} + \mathcal{F}_{G_1 G_2} + \mathcal{F}_{G_2 \bar{Q}_2} \right) d\sigma_4^{\text{LO}}. \tag{A.54}$$

A.5.3 Virtual contribution

From ref. [7], the matrix elements for the leading colour one-loop contribution to the $q\bar{q}gg$ final state for this colour ordering can be written in terms of a pole structure in ϵ multiplying the lowest order matrix elements and a function $\hat{\mathcal{L}}_A$ that is finite as $\epsilon \rightarrow 0$,

$$\mathcal{L}_A(G_1, G_2) = V(Q_1; G_1, G_2; \bar{Q}_2) \left| \mathcal{S}_\mu(Q_1; G_1, G_2; \bar{Q}_2) V^\mu \right|^2 + \hat{\mathcal{L}}_A(G_1, G_2). \tag{A.55}$$

The divergent factor V is given by,

$$V(Q_1; G_1, G_2; \bar{Q}_2) = \left(\frac{\alpha_s N}{2\pi} \right) \left(-\frac{\mathcal{P}(s_{Q_1 G_1})}{\epsilon^2} - \frac{\mathcal{P}(s_{G_2 \bar{Q}_2})}{\epsilon^2} - \frac{\mathcal{P}(s_{G_1 G_2})}{\epsilon^2} - \frac{3}{2} \frac{\mathcal{P}(Q^2)}{\epsilon} \right) \tag{A.56}$$

where we have introduced the notation,

$$\mathcal{P}(s) = \left(\frac{4\pi\mu^2}{-s} \right)^\epsilon \frac{\Gamma^2(1-\epsilon)\Gamma(1+\epsilon)}{\Gamma(1-2\epsilon)}. \tag{A.57}$$

In terms of cross sections, we have,

$$d\sigma_4^{\text{V}} = V(Q_1; G_1, G_2; \bar{Q}_2) d\sigma_4^{\text{LO}} + d\sigma_4^{\text{V,finite}}, \tag{A.58}$$

with,

$$\frac{d\sigma_4^{\text{V,finite}}}{\sigma_0} = \frac{(2\pi)^5}{s} \left(\frac{N^2 - 1}{N^2} \right) \left(\frac{\alpha_s N}{2\pi} \right)^3 \hat{\mathcal{L}}_A(G_1, G_2) \mathcal{J}_{(4)} dPS(Q^2; p_{Q_1}, p_{G_1}, p_{G_2}, p_{\bar{Q}_2}) \tag{A.59}$$

Here $\hat{\mathcal{L}}_A$ is a finite function given in terms of that logarithms and dilogarithms that arise in evaluating the one-loop contributions.⁷ We have ensured that the kinematic singularity structure of $\hat{\mathcal{L}}_A$ matches that of the tree-level $|\mathcal{S}_\mu(Q_1; G_1, G_2; \overline{Q}_2)V^\mu|^2$. It can be written symbolically as,

$$\hat{\mathcal{L}}_A = \sum_i P_i(s) L_i, \quad (\text{A.60})$$

where the coefficients $P_i(s)$ are rational polynomials of invariants. The finite functions L_i are the linear combinations of scalar integrals defined in [7] which are well-behaved in all kinematic limits, so that $\hat{\mathcal{L}}_A$ is numerically stable. Unfortunately, the analytic expression for $\hat{\mathcal{L}}_A$ is rather lengthy so we do not reproduce it here.

A.5.4 Next-to-leading order cross section

Assembling the various pieces, and applying coupling constant renormalisation,

$$\left(\frac{\alpha_s}{2\pi}\right) \rightarrow \left(\frac{\alpha_s(\mu)}{2\pi}\right) \left(1 - b_0 \left(\frac{\alpha_s(\mu)}{2\pi}\right) \frac{(4\pi)^\epsilon}{\epsilon\Gamma(1-\epsilon)}\right), \quad (\text{A.61})$$

the NLO four parton contribution is,

$$\begin{aligned} d\sigma_4^{\text{NLO}} &= d\sigma_4^V + d\sigma_4^{\text{sub}} + d\sigma_4^{\text{slice}} \\ &= K(Q_1; G_1, G_2; \overline{Q}_2) d\sigma_4^{\text{LO}} + d\sigma_4^{V, \text{finite}}, \end{aligned} \quad (\text{A.62})$$

where $d\sigma_4^{\text{LO}}$ and $d\sigma_4^{V, \text{finite}}$ are given by eqs. (A.49) and (A.59) respectively with the replacement $\alpha_s \rightarrow \alpha_s(\mu)$. The factor K is the sum of the divergent one loop factor (eq. (A.56)), the slicing factor (eq. (A.53)) and the subtraction term (eq. (A.54)),

$$\begin{aligned} K(Q_1; G_1, G_2; \overline{Q}_2) &= V(Q_1; G_1, G_2; \overline{Q}_2) + R(Q_1; G_1, G_2; \overline{Q}_2) \\ &\quad + \mathcal{F}_{Q_1 G_1}(s_{Q_1 G_1}) + \mathcal{F}_{G_1 G_2}(s_{G_1 G_2}) + \mathcal{F}_{G_2 \overline{Q}_2}(s_{G_2 \overline{Q}_2}) \\ &= \left(\frac{\alpha_s(\mu)N}{2\pi}\right) \left(\frac{197}{18} + \frac{\pi^2}{2}\right. \\ &\quad + \mathcal{F}_{Q_1 G_1}^\Delta\left(\frac{\Delta}{s_{Q_1 G_1}}\right) + \mathcal{F}_{G_1 G_2}^\Delta\left(\frac{\Delta}{s_{G_1 G_2}}\right) + \mathcal{F}_{G_2 \overline{Q}_2}^\Delta\left(\frac{\Delta}{s_{G_2 \overline{Q}_2}}\right) \\ &\quad - \frac{10}{6} \log\left(\frac{s_{Q_1 G_1}}{Q^2}\right) - \frac{11}{6} \log\left(\frac{s_{G_1 G_2}}{Q^2}\right) - \frac{10}{6} \log\left(\frac{s_{G_2 \overline{Q}_2}}{Q^2}\right) \\ &\quad \left. + \left(\frac{\alpha_s(\mu)}{2\pi}\right) 2b_0 \log\left(\frac{\mu^2}{Q^2}\right)\right). \end{aligned} \quad (\text{A.63})$$

Similarly, the five parton leading colour contribution to four jet-like observables is obtained from eqs. (A.51) and (A.53),

$$d\sigma_5^{\text{NLO}} = d\sigma_5 - d\sigma_5^{\text{sub}}, \quad (\text{A.64})$$

⁷Note that $\hat{\mathcal{L}}_A$ defined here is a factor of 8 smaller than that in [7].

evaluated with the running $\alpha_s(\mu)$. By construction this is finite as any one particle becomes unresolved. In the slicing regions, $d\sigma_5^{\text{NLO}} = 0$, while the phase space regions over which the subtraction terms are applied are implicit in the definition of the antenna functions.

Note that the four-dimensional limit of all cross sections may be taken with impunity now that the singularities have cancelled. Furthermore, there is no dependence in K on the slicing parameter δ which may also be taken as small as desired. The subtraction parameter Δ remains, and both $d\sigma_4^{\text{NLO}}$ and $d\sigma_5^{\text{NLO}}$ individually depend on it. However, the sum of both contributions is independent of the choice of Δ . The precise value of Δ can be made bearing in mind the numerical stability and speed of the final computer code. For small Δ , there may be sizeable cancellations between the four and five parton contributions, while for large Δ more CPU time is required to evaluate the subtraction terms. For our numerical results, we have taken,

$$\delta = 10^{-8}, \quad \Delta = 10^{-3}. \quad (\text{A.65})$$

References

- [1] R.K. Ellis, D.A. Ross and A.E. Terrano, Nucl. Phys. **B178** (1981) 421.
- [2] K. Fabricius, I. Schmitt, G. Kramer and G. Schierholz, Z. Phys. **C11** (1981) 315.
- [3] Z. Kunszt, P. Nason, G. Marchesini and B.R. Webber, in *Z Physics at LEP 1*, vol. 1, ed. G. Altarelli, R. Kleiss and C. Verzegnassi, CERN Yellow Report 89-08.
- [4] See for example, M. Schmelling, Proc. 28th International Conference on High Energy Physics, Warsaw, Poland, July 1996, Eds. Z. Ajduk and A.K. Wroblewski, World Scientific 1997, p91.
- [5] P.A. Movilla Fernández, O. Biebel, S. Bethke, S. Kluth, P. Pfeifenschneider and the JADE Collaboration, E. Phys. J. **C1** (1998) 461 [hep-ex/970834];
J.M. Campbell, E.W.N. Glover and C.J. Maxwell, Phys. Rev. Letts. **81** (1998) 1568 [hep-ph/9803254].
- [6] B. Adeva et al., L3 Collaboration, Phys. Lett. **B248** (1990) 227;
P. Abreu et al., DELPHI Collaboration, Phys. Lett. **B255** (1991) 466; Z. Phys. **C59** (1993) 357;
R. Akers et al., OPAL Collaboration, Z. Phys. **C65** (1995) 367;
D. Decamp et al., ALEPH Collaboration, Phys. Lett. **B284** (1992) 151;
R. Barate et al., ALEPH Collaboration, Z. Phys. **C76** (1997) 1.
- [7] E.W.N. Glover and D.J. Miller, Phys. Lett. **B396** (1997) 257 [hep-ph/9609474];
J.M. Campbell, E.W.N. Glover and D.J. Miller, Phys. Lett. **B409** (1997) 503 [hep-ph/9706297].
- [8] Z. Bern, L. Dixon and D.A. Kosower, Nucl. Phys. Proc. Suppl. **51C** (1996) 243 [hep-ph/9606378]; Z. Bern, L. Dixon, D.A. Kosower and S. Weinzierl, Nucl. Phys. **B489**

- (1997) 3 [hep-ph/9610370]; Z. Bern, L. Dixon and D.A. Kosower, Nucl. Phys. **B513** (1998) 3 [hep-ph/9708239].
- [9] K. Hagiwara and D. Zeppenfeld, Nucl. Phys. **B313** (1989) 560;
F. A. Berends, W. T. Giele and H. Kuijf, Nucl. Phys. **B321** (1989) 39;
N. K. Falk, D. Graudenz and G. Kramer, Nucl. Phys. **B328** (1989) 317.
- [10] A. Signer and L. Dixon, Phys. Rev. Lett. **78** (1997) 811 [hep-ph/9609460]; A. Signer and L. Dixon, Phys. Rev. **D56** (1997) 4031 [hep-ph/9706285]; A. Signer, Comput. Phys. Comm. **106** (1997) 125; A. Signer, Proceedings of 32nd Rencontres de Moriond: QCD and High-Energy Hadronic Interactions, p 211 (1997) March 1997 [hep-ph/9705218].
- [11] Z. Nagy and Z. Trócsányi, Phys. Rev. Lett. **79** (1997) 3604 [hep-ph/9707309];
Nucl. Phys. B, Proc. Suppl. **64** (1998) 63 [hep-ph/9708344];
‘Next-to-leading order calculation of four-jet observables in electron positron annihilation’, hep-ph/9806317;
‘Multijet rates in e^+e^- annihilation: perturbation theory versus LEP data’, hep-ph/9808364.
- [12] Z. Nagy and Z. Trócsányi, Phys. Lett. **B414** (1997) 187 [hep-ph/9708342].
- [13] Z. Nagy and Z. Trócsányi, Phys. Rev. **D57** (1998) 5793 [hep-ph/9712385].
- [14] J.G. Körner, G. Schierholz and J. Willrodt, Nucl. Phys. **B185** (1981) 365;
O. Nachtmann and A. Reiter, Z. Phys. **C16** (1982) 45;
M. Bengtsson and P.M. Zerwas, Phys. Lett. **B208** (1988) 306.
- [15] Z. Nagy and Z. Trócsányi, ‘Excluding light gluinos using four-jet LEP events: a next-to-leading order result’, hep-ph/970343.
- [16] S. Frixione, Z. Kunszt and A. Signer, Nucl Phys. **B467** (1996) 399 [hep-ph/9512328];
Z. Nagy and Z. Trócsányi, Nucl. Phys. **B486** (1997) 189.
- [17] S. Catani and M.H. Seymour, Phys. Lett. **B378** (1996) 287; Nucl. Phys. **B485** (1997) 291.
- [18] W.T. Giele and E.W.N. Glover, Phys. Rev. **D46** (1992) 1980.
- [19] E.W.N. Glover and M.R. Sutton, Phys. Lett. **B342** (1995) 375 [hep-ph/9410234];
A. Gerhmann-De Ridder and E.W.N. Glover, Nucl. Phys. **B517** (1998) 269 [hep-ph/9707224].
- [20] The fortran code for EERAD2 is available by email from E.W.N.Glover@durham.ac.uk or via the web-page <http://qcd2.dur.ac.uk/EERAD2.html>.
- [21] E.W.N. Glover, hep-ph/9805481, to appear in Proceedings of 33rd Rencontres de Moriond: QCD and High-Energy Hadronic Interactions, March 1998.
- [22] G. Parisi, Phys. Lett. **B74** (1978) 65.

- [23] S. Brand et al, Phys. Lett. **12** (1964) 57;
E. Farhi, Phys. Rev. Lett. **39** (1977) 1587.
- [24] L. Clavelli, Phys. Lett. **B85** (1979) 111.
- [25] S. Catani, G. Turnock, B.R. Webber, Phys. Lett. **B295** (1992) 269.
- [26] J.D. Bjorken, S. Brodsky, Phys. Rev. **D51** (1970) 1416.
- [27] JADE Collaboration, W. Bartel et al, Z. Phys. **C33** (1986) 23;
JADE Collaboration, S. Bethke et al, Phys. Lett. **B213** (1988) 235.
- [28] Yu.L. Dokshitzer, Contribution to the Workshop on Jets at LEP and HERA, J. Phys. **G17** (1991) 1441;
S. Catani, Yu.L. Dokshitzer, M. Olsson, G. Turnock and B.R. Webber, Phys. Lett. **B269** (1991) 491.
- [29] S. Bethke, Z. Kunszt, D.E. Soper and W.J. Stirling, Nucl. Phys. **B370** (1992) 310 and hep-ph/9803267.
- [30] G. Grunberg, Phys. Lett. **B95** (1980) 70; Phys. Rev. **D29** (1984) 2315.
- [31] P. M. Stevenson, Phys. Rev. **D23** (1981) 2916.
- [32] S. Catani, G. Turnock, B.R. Webber, L. Trentadue, Phys. Lett. **B263** (1991) 461; Nucl. Phys. **B407** (1993) 3;
S. Catani, G. Turnock, B.R. Webber, Phys. Lett. **B272** (1991) 368; Phys. Lett. **B295** (1992) 269;
S. Catani and B.R. Webber, hep-ph/9801350.
- [33] P. Abreu et al, DELPHI Collaboration, Z. Phys. **C73** (1996) 11.
- [34] R.M. Barnett et al, Phys. Rev. **D54** (1996) 1 and 1997 off-year partial update from <http://pdg.lbl.gov>.
- [35] C.J. Maxwell, ‘Complete renormalisation group improvement of QCD perturbation theory’, hep-ph/9809270.
- [36] B.R. Webber, Phys. Lett. **B339** (1994) 148;
B.R. Webber, *Proc. Summer School on Hadronic Aspects of Collider Physics, Zuoz, Switzerland, 1994* [hep-ph/9411384];
G.P. Korchemsky and G. Sterman, Nucl. Phys. **B437** (1995) 415;
G.P. Korchemsky and G. Sterman, *Proc. 30th Rencontres de Moriond, Les Arcs, France, 1995* [hep-ph/9505391];
P. Nason and M.H. Seymour, Nucl. Phys. **B454** (1995) 291;
R. Akhoury and V.I. Zakharov, Phys. Lett. **B357** (1995) 646;
R. Akhoury and V.I. Zakharov, Nucl. Phys. **B465** (1996) 295.

- [37] Yu.L. Dokshitser and B.R. Webber, Phys. Lett. **B352** (1995) 451 [hep-ph/9504219];
Phys. Lett. **B404** (1997) 321 [hep-ph/9704298];
Yu.L. Dokshitser, G. Marchesini and B.R. Webber, Nucl. Phys. **B469** (1996) 93 [hep-ph/9512336].
- [38] Z. Kunszt and D.E. Soper, Phys. Rev. **D46** (1992) 196.
- [39] J.M. Campbell and E.W.N. Glover, Nucl. Phys. **B527** (1998) 264 [hep-ph/9710255].
- [40] J.M. Campbell, Ph.D. thesis, ‘Higher Order Corrections to Multijet Production in e^+e^- Annihilation’, Durham (1998).
- [41] G. Altarelli and G. Parisi, Nucl. Phys. **B126** (1977) 298.
- [42] D. Kosower, Phys. Rev. **D57** (1998) 541 [hep-ph/9710213].